Dynamic modes of Notch transcription hubs conferring memory and stochastic activation revealed by live imaging the co-activator Mastermind.

Authors:
F Javier deHaro-Arbona[1], Charalambos Roussos[1], Sarah Baloul[1], Jonathan Townson[1], Maria J. Gomez-Lamarca[1, 2], Sarah Bray[1, *].

Affiliations:

1. Department of Physiology Development and Neuroscience
   University of Cambridge,
   Downing Street,
   Cambridge, CB2 3DY, UK

2. Instituto de Biomedicina de Sevilla (IBiS), Hospital Universitario Virgen del Rocío/CSIC/Universidad de Sevilla, Departamento de Biología Celular, 41013 Seville, Spain

*Corresponding author and lead contact: sjb32@cam.ac.uk

Summary

Developmental programming involves the accurate conversion of signaling levels and dynamics to transcriptional outputs. The transcriptional relay in the Notch pathway relies on nuclear complexes containing the coactivator Mastermind (Mam). By tracking these complexes in real time, we reveal that they promote formation of a dynamic transcription hub in Notch-ON nuclei which concentrates key factors including Mediator CDK module. The composition of the hub is labile and persists after Notch withdrawal conferring a memory that enables rapid reformation. Surprisingly, only a third of Notch-ON hubs progress to a state with nascent transcription, that correlates with Polymerase II and core Mediator recruitment. The probability is increased by a second signal. The discovery that target-gene transcription is probabilistic has far-reaching implications because it implies that stochastic differences in Notch pathway output can arise downstream of receptor activation.

Keywords: Notch signaling, Mastermind, Transcription, Live-imaging, Mediator Complex, Drosophila

Introduction

Cells face the challenge of transmitting information accurately, so that cell-surface signals are translated into correct transcriptional responses, and how this is achieved mechanistically remains a major question. Notch is a key signalling pathway that leads to gene activation when ligand and receptor engage upon cell contact [1–3]. The physical interaction brings about a conformational change that permits proteolytic cleavage and release of Notch Intra Cellular Domain (NICD) [4–6]. This moiety forms a complex with CSL (CBF-1/RBPJ-κ in mammals, Suppressor of Hairless in *Drosophila* and LAG-1 in *C. elegans*), a transcription factor that binds to specific DNA motifs, and Mastermind (Mam) a co-activator [7–9]. This tripartite activation complex promotes transcription from the target genes where it is recruited. The sites of recruitment differ according to the cellular context, resulting in different transcriptional outcomes and suggesting that other factors are important in preparing the targets for activation [10]. In addition, release of NICD brings about rapid and robust transcriptional responses within minutes, raising the question how the molecules of cleaved Notch achieve this so efficiently [11–13].

Regulation of transcription must be tightly controlled in space, time, and genomic location [14,15]. Many different studies report that sequence-specific transcription factors, key coactivators, and RNA polymerase II (PolII) itself undergo dynamic clustering within a nucleus [16–19]. Clustering appears to be mediated by a combination of specific structure-mediated interactions (e.g. DNA-binding, protein-protein interactions) and multivalent interactions among intrinsically disordered regions (IDRs) present in most transcription factors [20,21]. In this way, transcription is regulated by the formation of functionally specialized local protein microenvironments or transcription "hubs" associated with target enhancers [22]. In some cases, these have the properties of 'condensates' whose formation and dissolution has been explained by the process of phase separation [23]. As the resulting assembly is non-stoichiometric, it may enable a small number of transcription factor molecules to drive productive transcription. Such a mechanism could thus explain how NICD, whose nuclear levels are frequently below the level of detection *in vivo*, can successfully promote robust-target gene transcription

[24]. Indeed, all members of the Notch activator complex contain unstructured regions that could contribute to the assembly of a hub.

The formation of the tripartite Notch activator complex involves a conserved helix in the N-terminal region of Mam proteins which is responsible for the direct interactions with CSL and NICD [8,9]. The remainder of the large Mam proteins are poorly conserved and appear to be predominantly unstructured albeit to have potential roles in recruiting other cofactors [25,26]. For example, there is evidence that human MAML1 interacts with the histone acetyl transferase CBP/p300, which is present at Notch regulated enhancers in genome-wide studies [26–28], and whose recruitment is implicated in activating some targets [29,30]. The C-terminal portion of MAML1 is also suggested to recruit CDK8, the enzymatic core of the Mediator kinase module [31–33]. What role these factors play in the recruitment, dynamics and assembly of functional Notch transcription assemblies, and whether these acquire hub-like properties is unclear.

Live imaging of endogenously tagged proteins offers a non-invasive approach to probe the assembly and composition of transcription hubs *in vivo*. Using this strategy, we have previously shown that CSL is recruited in a very dynamic manner to a target genomic locus *in vivo* [34]. However, as CSL exists in both corepressor and co-activator complexes [35], the extent that these dynamics reflect the characteristics of the activation complex remains to be established. Here we incorporated fluorescent tags into the endogenous Mam protein to investigate the behaviours of this Notch nuclear co-activator *in vivo*, in combination with a method for live-imaging of a target genomic locus that responds robustly to Notch activation. The emerging model is that Notch activity leads to the formation of 'transcription hubs' that exist in different states. When Mam is present, key components of the transcriptional machinery become locally concentrated but, surprisingly, in the absence of synergising factors, the conversion to productive transcription only occurs stochastically. In addition, the open chromatin state that is generated decays slowly after Notch withdrawal, providing a memory that enables a more rapid response to a subsequent round of Notch activation.

Results

Dynamics of Mastermind recruitment in relation to its partner CSL

The Mam coactivator is an integral part of the Notch transcription complex [8,9,30,36]. To track Mam dynamic behaviours *in vivo* we inserted GFP or Halo into the N-terminus of the endogenous Mam using CRISPR-Cas9 genome editing [34]. The resulting flies are homozygous viable with no evident phenotypes, indicating that the tagged Mam proteins are fully functional. We first set out to compare the recruitment and dynamics of CSL and Mam at a target locus in Notch-OFF and Notch-ON conditions, taking advantage of *Drosophila* salivary glands, where the polytene (multiple copy) chromosomes aid detection of chromatin-associated complexes. We used the Int/ParB system, where fluorescently labelled ParB proteins bind to inserted Int sequences, to detect the well- characterised *Enhancer of split complex* [*E(spl)-C*], which contains multiple Notch-regulated genes[34]. Because of the aligned copies of the genome in the polytene chromosomes, the target genomic locus appears as an easily distinguished fluorescent "band" in each nucleus during live imaging (Figure 1A).

The Notch pathway is normally inactive in salivary glands, providing a baseline Notch-OFF condition. This was converted to Notch-ON by the expression of a constitutively active form of Notch, NΔECD, using the GAL4-UAS system which allows tissue-specific and temporal control. Because it lacks the extracellular domain, NΔECD is constitutively cleaved by gamma-secretase to release NICD, mimicking ligand induced activation [37–39]. Comparing the localization of GFP::Mam in Notch-OFF and Notch-ON conditions, it was immediately evident that Mam was robustly recruited to *E(spl)-C* in Notch-ON conditions in a similar manner to CSL [34]. In Notch-OFF conditions, both proteins were diffuse throughout the nucleus, with a low level of CSL, but not Mam, present at *E(spl)-C*. In Notch-ON conditions, strong enrichment of both Mam and CSL was consistently detected around *E(spl)-C* (Figure 1B).

To compare the dynamics of Mam and CSL at *E(spl)-C* in Notch-ON conditions, we performed Fluorescence Recovery After Photobleaching (FRAP) focussed on the region defined by the locus-tag. Unlike CSL, which had a rapid recovery (t1/2=9 secs),

Mam exhibited much slower dynamics (t1/2=40 secs) and failed to fully recover over the time-course of the experiment (Figure 1C). Slower recovery can arise from higher proportion of bound molecules, longer residence times and/or slower diffusion coefficients[40]. The results therefore suggest that the Mam-containing activation complexes have different properties from the majority of CSL complexes.

The other main partner for CSL in *Drosophila* is the corepressor Hairless. In FRAP experiments Hairless has a fast recovery, with a profile close to that of CSL (Figure 1C), consistent with a significant fraction of CSL being complexed with Hairless even in Notch-ON conditions[34]. The difference in dynamics between CSL and Mam could therefore be explained by the former being involved in two different complexes with different dynamics. To test this, we depleted Hairless using RNAi-mediated knock-down and measured the effects on enrichment and dynamics of CSL and Mam. As expected, Mam recruitment levels and the dynamics measured by FRAP were unchanged (Figure 1C', S1B). In contrast, CSL levels and recruitment were reduced and its FRAP recovery was slowed, albeit not to the extent that it recapitulated the Mam profile (Figure 1C', S1C). Together the results indicate that the activation complexes, containing CSL and Mam, have slower dynamics than the repressor complexes, containing CSL and Hairless, and that the recovery of CSL reflects its participation in the two types of complexes.

To further investigate the dynamics of Mam and CSL complexes, we performed single particle tracking (SPT) by sparse labelling of endogenous Halo::Mam and Halo::CSL in live tissue [41,42]. Gaussian fitting-based localisation and Multiple hypothesis tracking were used for detection and tracking of single particles within the nucleus with a ~20nm precision[34] . Using a Bayesian treatment of Hidden Markov Model, vbSPT [43], trajectories were assigned into 2 states, defined by a Brownian motion diffusion coefficient, that correspond to bound (diffusion coefficient 0.01$\mu m^2/s$) versus more freely diffusing complexes (diffusion coefficient >0.25$\mu m^2/s$) (Figure S1D). A greater proportion (53%) of Mam complexes were in the bound state than CSL complexes (39%), consistent with the differences between their FRAP curves. We also analysed the density of particle trajectories in relation to the *E(spl)*-C locus in Notch-OFF and

Notch-ON conditions. In comparison to their average distribution across the nucleus, both CSL and Mam trajectories were significantly enriched in a region of approximately 0.5 µm around the target locus in Notch-ON conditions, reflecting robust Notch dependant recruitment to this gene complex.

To assess whether Mam complexes have longer residence times once recruited to the chromatin, we analyzed the duration of trajectories for Mam, CSL and Hairless. Long trajectories correlate to bound complexes, because faster moving particles are rapidly lost from the field of view, and the length of time they are detectable is an indication of relative residence times. There were clear differences between the trajectory durations for Mam, CSL and Hairless. Mam trajectories had the longest durations of up to 15 secs, Hairless trajectories were the shortest (up to 5-7 secs) and CSL trajectories were intermediate (up to 10 secs) (Figure 1E). The differences were recapitulated when only the trajectories in the region around *E(spl)-C* were analysed (Figure 1E'). The residences are likely an underestimation because bleaching and other technical limitations also affect the track durations[44]. Nevertheless, these data confirm that Mam-containing complexes have on average longer residence times than other CSL complexes which, together with the higher proportion of bound molecules overall, explains the slower recovery dynamics measured by FRAP.

The fact that CSL dynamics, measured by FRAP and SPT, are intermediate between Hairless and Mam fit well with it being present in two types of complexes [co-activator (Mam) and corepressor (Hairless)]. However, whether the contribution from CSL co-repressor complexes can fully explain all the observed differences between CSL and Mam is not fully clear. First, when we depleted Hairless, so that the majority of CSL present would be in co-activator complexes, CSL FRAP recovery curves were still substantially different from those of Mam. Second, none of the CSL trajectories had a duration approximating those of the longest Mam trajectories, despite that over 50,000 CSL trajectories were tracked (compared to 14,000 Mam, Figure S1D). It is possible therefore that, once recruited, Mam can be retained at target loci independently of CSL by interactions with other factors so that it resides for longer.

Hub-like properties of CSL-Mastermind complexes in Notch active cells

The enrichment of CSL and Mam around *E(spl)-C* that we detect by live-imaging is not unexpected because this locus has multiple genes containing CSL binding-motifs [34,45]. However, the diffuse enrichment was not maintained when the tissues were fixed, a characteristic reported for proteins present in condensate-like hubs [46] (Figure S2A). The localized concentration of exchanging CSL and Mam complexes around *E(spl)-C* in Notch-ON nuclei may therefore have properties of a transcription hub, with some of the recruitment being reliant on weak interactions mediated by low-complexity regions [47–49].

First, we asked to what extent CSL recruitment was correlated with the number of CSL binding motifs. To do so, we took advantage of fly strains containing multiple copies of CSL motifs inserted at an ectopic position in the genome [50] and compared the recruitment with insertions containing 12 or 48 CSL motifs. In Notch-ON conditions, these insertions were sufficient to generate an ectopic band of CSL recruitment similar to the native *E(spl)-C* (Figure 2A). Remarkably the amounts of CSL recruited to loci with 12 and 48 ectopic sites were almost identical. Thus, there is not a direct correlation between the number of motifs and the amount of CSL recruited under these conditions. Nor does it appear that the amounts of CSL complexes are a limiting factor as there was no decrease in recruitment at the endogenous *E(spl)-C* locus, even in nuclei with a 48 CSL-motif insertion.

Second, we questioned whether the non-stochiometric recruitment of activator complexes to loci with CSL motifs might involve additional weak protein-protein interactions between some components, as observed in several transcription hubs where intrinsically disordered protein domains play a part [20,51]. We used Intrinsically Disordered Region (IDR) prediction algorithms [52] to identify IDRs within NICD, CSL, Mam and Mediator1 (Med1, part of the mediator complex) (Figure 2B) and generated transgenic flies where each IDR was expressed as a fusion with GFP. The recruitment of the IDR::GFP fusions to *E(spl)-C* was then measured in Notch-ON and OFF conditions (Figure 2C). Of the IDRs tested, the C-terminal region from NICD was the

most strongly enriched at *E(spl)-C* in Notch-ON conditions. A very low level of enrichment was evident for a shorter NICD fragment, that lacked the C-terminal PEST sequences, for the CSL C-terminus and for Med 1 IDR. Surprisingly, little or no enrichments occurred with Mam-IDRs, despite that this large protein has been reported to interact with p300 and other factors (Figure S2B). Notably, Mam-nIDR::GFP fusion was present in droplets, suggesting it can self-associate when present in a high local concentration (Figure S2B, [53]). Our results suggest therefore that the IDR in NICD may contribute to the localized enrichments at target loci in Notch-ON cells, potentially in combination with IDRs present in other recruited factors. In support of this hypothesis, deletion of the IDR from NICD led to a reduction in the levels and stability of Mam recruitment to *E(spl)*-C (Figure 2D).

Third, we reasoned that the presence of a transcription hub, where complexes are retained in the vicinity via protein interactions, should result in local changes in the behaviours of CSL and Mam. After segregating the SPT trajectories according to their diffusion properties as described above (Figure S2D), we analyzed the spatial distribution of the slow and fast populations in relation to the *E(spl)-C*, defined as the area within 550nm of the locus-tag. Based on the shape and centre of this region, concentric zones were defined at 550nm distances and the proportions of slow- and fast-moving particles in each zone were calculated. The results show that there is an enrichment for slow-diffusing and a depletion of fast-moving particles close to the locus, with these altered properties extending to a region of up to 1µm away (Figure 2E).

Together our data support the model that CSL-Mam complexes are recruited and form a hub of high protein concentrations around the target locus in Notch-ON conditions and suggest that IDR interactions, as well as DNA binding, contribute to their recruitment and retention in a region surrounding the active enhancers.

Mediator CDK module is required for stable Mastermind recruitment.

The hub-like properties and slower turnover of Mam complexes compared to CSL suggest that other factors will be involved in their stabilization. We therefore tested

the consequences of inhibiting or depleting different factors to distinguish those required for Mam enrichment at *E(spl)-C* in Notch-ON nuclei. We first asked whether active transcription was required for Mam recruitment, by exposing the tissue to a specific inhibitor of transcription initiation, triptolide [54]. No change in Mam enrichment or recovery was detected, arguing that Mam recruitment is not dependent on initiation or RNA production (Figure 3A, B). As previous studies have reported an interaction between Mam and the histone acetylase CBP/p300 [30,33,55,56], we next inhibited CBP activity using a potent and selective inhibitor A485 [57]. Tissues were exposed to A485 for one hour which was sufficient to severely reduce the levels of H3K27Ac and *E(spl)m3* transcription, indicating that the treatment was effective (Figure 3C, S3A-B). Surprisingly however, there was no change in the recruitment of Mam in these conditions (Figure 3C). We also depleted CBP by RNAi and, as with the drug treatment, Mam recruitment was unchanged (Figure 3D). Based on these results, we conclude that CBP is not essential for the recruitment of Mam complexes to the hub formed at the *E(spl)-C* locus.

As several studies have suggested that the Mediator CDK module, containing Med12, Med 13, CDK8 and CycC, influences Notch dependent transcription, we next focused on the role of this complex [31,32,58]. First, we depleted Med13 and CDK8 using validated RNAi lines [59,60]. Med13 depletion led to a loss of *E(spl)*m3 transcription, confirming its role (Figure S3D). In these conditions we detected a substantial reduction in Mam recruitment to *E(spl)-C* in Notch-ON cells, suggesting the CDK module plays a role in retaining Mam at target sites (Figure 3E, G). Second, we incubated the tissues in Senexin B or Senexin A, two drugs that target CDK8 activity [61,62] for 1 hour prior to imaging. In both cases the treatment was sufficient to significantly impair Mam levels at *E(spl)-C* (Figure 3F, S3C) while a CDK9 inhibitor, NVP2, had no effect in the same assays (Figure S3E-F). Third we investigated whether CDK module was recruited to *E(spl)-C*, in Notch-ON nuclei using an existing line in which YFP is fused to Med13 [63,64]. Significant enrichment of Med13::YFP was detected at *E(spl)-C* in Notch-ON nuclei, (Figure 3H) demonstrating that it is present in the hub with Mam.

Despite their effects on Mam recruitment, neither depletion of Med13 or CDK8 nor Senexin treatments caused any significant reduction in the levels of CSL recruited. On the contrary, a small increase occurred (Figure 3E, F). The differences in the effects on Mam and CSL imply that the CDK module is specifically involved in retaining Mam in the hub, and that in its absence other CSL complexes "win-out", either because the altered conditions favour them and/or because they are the more abundant.

Mastermind is not essential for chromatin accessibility.

The observed differences between CSL and Mam in their dynamics and dependency on CDK module led us to speculate that they make different functional contributions to the transcription hub. To probe the role of Mam, we examined the consequences when its recruitment to the complex was prevented. The N-terminal peptide from Mam functions as a dominant negative (MamDN) by occupying the groove formed by CSL-NICD and, when overexpressed, prevents transcription of target genes [8,9,65]. As predicted, MamDN expression in Notch-ON conditions prevented recruitment of full-length Mam to *E(spl)-C* (Figure 4A). To verify that MamDN also inhibited transcription under these conditions, we used single molecule Fluorescent in situ hybridization (smFISH) with probes targeting *E(spl)-C* transcripts that are robustly up-regulated in this tissue [34]. Nascent transcripts of *E(spl)m3* were detected at *E(spl)-C* in Notch-ON nuclei and were at very reduced levels in nuclei co-expressing MamDN (Figure 4B) confirming that target-gene transcription is blocked.

By contrast, recruitment of CSL was unaffected by MamDN expression. It was robustly recruited to *E(spl)-C* at a similar level to untreated Notch-ON nuclei despite the absence of full length Mam (Figure 4A' [34]). Identical results were obtained when Mam was depleted by RNAi (Figure S4A [34]). The fact that CSL was still strongly enriched under these conditions argues that some of the Notch induced changes at *E(spl)-C* occur independently of the co-activator, as proposed previously [34]. In contrast to CSL, the enrichment of Med13 was lost in the presence of MamDN revealing that Med13 recruitment requires Mam, as well as the converse (Figure 4C).

Since MamDN does not prevent CSL recruitment, although it blocks recruitment of Med13 and transcription, we hypothesised that some Notch-induced effects at target enhancers may not require Mam. One consequence from Notch activation is an increase in chromatin accessibility at sites where CSL is recruited [34,66]. We therefore asked whether changes in chromatin accessibility still occur in the presence of MamDN by performing ATAC and analysing by qPCR the accessibility of the regulatory regions abutting *E(spl)mβ* and *E(spl)m3*[34]. Both regions significantly increased in accessibility in Notch-ON nuclei which was maintained in the presence of MamDN (Figure 4D, D'). In addition, we found that the levels of GFP::NICD-IDR recruited to *E(spl)-C* were similar in the presence and absence of MamDN (Figure S4B), arguing that a modified hub is still formed.

Altogether these observations support the model that the increased chromatin accessibility elicited by Notch activation can occur independently of Mam and must rely on other functions conferred by CSL and NICD [34], while Mam is essential to recruit Mediator CDK module and enable transcription.

CSL recruitment and chromatin accessibility persist after Notch inactivation, conferring memory

Our results suggest that there are two or more separable steps involved in forming an active transcription hub in Notch-ON cells: a Mam-independent change in chromatin accessibility, a Mam-dependent recruitment of Mediator and initiation of transcription. If these are discrete steps, we reasoned that they might decay with different kinetics when Notch activity is removed. We took advantage of the thermosensitive Gal4/Gal80ts system to switch off Notch activity and assessed the consequences on CSL and Mam recruitment at two different time points: 4 hours and 8 hours after the switch-off. Imaging Mam::GFP and CSL::mCherry simultaneously, it was evident that Mam recruitment levels decreased more rapidly. CSL remained relatively constant through both time points while, in contrast, the levels of Mam at *E(spl)-C* decreased sharply after 4 hours (Figure 5A). Based on these results we propose that, after Notch

activity decays, the locus remains accessible because when Mam-containing complexes are lost they are replaced by other CSL complexes (e.g. co-repressor complexes).

As Notch removal leads to a loss of Mam, but not CSL, from the hub, it should recapitulate the effects of MamDN. We therefore measured the accessibility of target enhancers at *E(spl)mβ* and *E(spl)m3* at the 8-hour timepoint by ATAC. Neither enhancer exhibited any reduction in accessibility at this timepoint, consistent with the continued recruitment of CSL and the results obtained with MamDN (Figure 5B). In contrast, the gradual loss of Mam complexes was accompanied by reduced transcription, as detected by smFISH. Expression of *E(spl)m3* was already significantly reduced at 4 hours, when levels of nascent transcripts at *E(spl)-C* and of cytoplasmic transcripts had. both decreased (Figure 5C). By 8 hours both nascent and cytoplasmic *E(spl)m3* transcripts were almost undetectable (Figure 5C). Thus, the changes in transcription correlate well with the reduction in Mam recruitment whereas the chromatin accessibility persists in the absence of Mam.

We next tested whether target loci retain "memory" of previous Notch activation that would make them more receptive to a subsequent exposure to Notch activity. To do so, we took advantage of the temporal control provided by optogenetic release of NICD using OptIC-Notch{ω} [67]. We compared the response to Notch activation in cells that had been 'preactivated' with blue light and subsequently kept in the dark for a short period, and 'naïve' cells, which had been kept solely in the dark and hence had no prior Notch activity (Figure 5D). After 4h in the dark following the initial activation, we observed that CSL was retained at *E(spl)-C*, while Mam was depleted, similar to the temporal experiments above. During the subsequent activation and imaging, enrichment of Mam occurred much more rapidly in preactivated cells in comparison to naïve cells, suggesting the former preserve a memory of previous activation and are primed to rapidly reform an active hub containing Mam (Figure 5F).

Together, our data indicate that CSL recruitment and increased chromatin accessibility persist after Notch removal and after the loss of the Mam activation complexes. This

confers a memory state that enables rapid re-assembly of an activation hub in response to subsequent Notch activity.

Probability of transcription conferred by Mastermind.

When analyzing the smFISH data we noticed that, even in Notch-ON conditions, a fraction of nuclei lacked foci of nascent transcription at *E(spl)-C*. Since Mam was present at *E(spl)-C* in all nuclei (Figure 6A, S5A), this led us to question whether the presence of Mam-complexes was sufficient to recruit downstream factors required for transcription initiation. We therefore investigated the extent that RNA Pol II was recruited to *E(spl)-C* in Notch-ON cells, using endogenous GFP::Rbp3 [16]. When scanning all nuclei, it was evident that Rbp3 enrichment at *E(spl)-C* in Notch-ON cells was highly variable. Robust enrichment was detected in a subset of nuclei but, in other cases, there was little/no enrichment above nuclear levels (Figure S5B). Performing a Gaussian population fitting on the data, 2 populations gave the best fit and, based on these, 36% of nuclei had significant enrichment and 64% had similar levels to Notch-OFF (Figure 6B, S5B). This differs from Mam where all nuclei fall into a single population that has significant Mam enrichment at *E(spl)-C* (Figure 6A, S5A). The striking difference in the proportions of nuclei with Pol II and with Mam enrichment implies that there is a limiting step, which results in transcription initiation being probabilistic/stochastic in these conditions.

It has been suggested that the core Mediator complex, as distinct from the CDK module, has an important role in bridging between enhancer bound transcription complexes and initiation complexes at promoters [68–70]. To investigate core Mediator recruitment we generated a GFP::Med1 fusion by CRISPR genome-editing. Using this endogenously tagged protein, which is homozygous viable, we found that GFP::Med1 became enriched at *E(spl)-C* with a similar probability to Rbp3 (Figure 6C). Indeed when we compared directly the enrichment of Pol II and Med1 in Notch-ON nuclei, by using mCherry::Rbp1 [16] to monitor Pol II, we observed a significant correlation between the two proteins (R^2 = 0.69) (Fig 6E). No such correlation with CSL was observed, in the same experiments (Figures S5E).

To verify that only a subset of nuclei was transcriptionally active we used a strain where MS2 loops have been inserted into *E(spl)mβ* using CRISPR-Cas9 engineering [11] and imaged transcription live in Notch-ON nuclei. In the presence of MCP-GFP, which binds to MS2 loops in the RNAs produced, nascent sites of transcription appear as puncta that align into a band of fluorescence at *E(spl)-C*, due to the multiple aligned gene copies. A robust band of MCP/MS2 nascent transcription at *E(spl)-C* was detected in Notch-ON conditions, demonstrating that some nuclei were actively transcribing (Figure 6D, S5C). However, this was present in only a third (37%) of nuclei. These data show that only a subset of nuclei engage in active transcription, and that the proportion of active nuclei is similar to that with recruitment of Pol II and Med1.

These data demonstrate that presence of Mam-complexes is not sufficient to reliably drive all the steps required for transcription in every Notch-ON nucleus. Instead, it appears that transcription is initiated stochastically. This is unexpected and could only be detected because our *in vivo* live imaging approaches enable us to monitor the responses of individual nuclei.

Ecdysone cooperates with Notch to increase probability of transcription.

Even though relatively few Notch-ON nuclei became transcriptionally active in our experiments, they all had robust recruitment of Mam complexes and of Med13 at *E(spl)-C*. Thus, in many respects the gene locus becomes competent or poised for transcription in all nuclei. We wondered, therefore, whether the presence of a second stimulatory signal would increase the probability of loci becoming transcriptionally active. In normal development, salivary glands become exposed to the steroid hormone ecdysone a few hours after we perform our experiments. Two observations suggested that ecdysone was a good candidate for a cooperating signal. First, previous genome-wide studies detected ecdysone receptor binding in the *E(spl)-C* region [71]. Second, we noticed in rare samples containing an older gland, that it had a higher proportion of active nuclei. We therefore exposed the early-stage Notch-ON salivary glands to ecdysone and analyzed the proportion of nuclei with MS2/MCP puncta. Strikingly, the

proportion of active nuclei increased dramatically to 70% following ecdysone treatment. No such effects were seen in Notch-OFF nuclei where *E(spl)mβ* remained silent even after ecdysone treatment (Figure 6F).

We further tested the effect of ecdysone by measuring changes in enrichment of Pol II and Med1 at *E(spl)-C*. The proportion of nuclei with clear enrichment of each factor was significantly increased (Figure 6F). Thus, the switch from the more stochastic transcription elicited by recruitment of Mam alone to the more robust initiation when ecdysone was added, correlated with the presence of Med1 and Pol II. As Mediator is reported to stabilize enhancer-promoter interactions, its recruitment may be what limits the probability of transcription [68,72].

Discussion

Understanding the mechanisms by which signaling levels and dynamics are accurately converted to transcriptional outputs is fundamental for developmental programming. Here we used live imaging approaches to probe how this occurs in the context of the Notch pathway, where the transcriptional relay relies on the single NICD released by each activated receptor and the nuclear complexes it forms with its partners CSL and Mam. By tracking these complexes in real time we unveiled three important features (Figure 7): (i) in Notch-ON nuclei, the activation complexes promote formation of a dynamic protein hub at a regulated gene locus that concentrates key factors including Mediator CDK module, (ii) the composition of the hub is changeable and the footprint persists after Notch withdrawal conferring a memory that enables rapid reactivation, (iii) transcription is probabilistic in Notch-ON nuclei, such that only a third of nuclei with a hub are actively transcribing. This has far-reaching implications because it reveals that stochastic differences in Notch pathway output can arise downstream of receptor activation.

Notch transcription complexes form a hub

Many recent studies have demonstrated that hubs or condensates play key roles in gene-expression regulation by maintaining a high local concentration of transcription

factors and other regulatory complexes [17,22,47,68]. By tracking the co-activator Mam in real time, we show that Notch transcription complexes become enriched around a target locus in a zone that has characteristics of a hub. First, the high-concentration zones are highly dynamic and undergo a continual exchange between activator and repressor complexes. The former exhibit longer residence times, suggesting they are stabilised by other interactions. Second, recruitment of CSL-containing complexes is non-stoichiometric with respect to CSL-binding motifs and can in part be recapitulated by an IDR from NICD. Although deletion of the IDR biases against activation complex recruitment, our evidence suggests that individual IDRs make a minor contribution, as observed recently in an unbiased study of IDRs. Third, the enriched zone is readily detectable by live imaging, but is sensitive to fixation, as has been reported for some subcellular protein condensates [73]. Although transcription hubs have frequently been associated with phase separation, examples are emerging where high local concentrations of transcription factors can be achieved without it [21]. Similarly, the locally enriched Notch-induced hubs in our experiments do not manifest clear properties of liquid condensates despite being non-stoichiometric.

We propose that NICD and Mam participate in multivalent interactions which increase the likelihood of the tripartite activation complexes remaining in the chromatin-associated state and which facilitate recruitment of coactivators to form a local hub (Figure 7). The latter include subunits of CDK module, Med 13. We find that perturbations to CDK module compromise Mam levels in the hub and vice versa, highlighting its importance. Indeed, the CDK module has been reported to interact directly with Mam and to play a role in Notch signalling output [31,32], and recent studies in mammalian cells indicate CDK8 acts positively in signal-induced gene expression [74]. Although its recruitment is proposed to prepare genes for activation, the transition to activation necessitates CDK8 release, since CDK module sterically inhibits core Mediator-Pol II interactions[72,75]. This is consistent with our results showing that Med13 recruitment is highly dynamic and that, despite most nuclei showing Med13 enrichment within the hub, the probability of transcription is low, as discussed below.

Role of hub in conferring transcriptional memory

Assembly of the transcription hub at *E(spl)-C* depends on Notch activity but, surprisingly, can form in the absence of the co-activator Mam, albeit the composition differs. Notably, CSL complexes continue to be highly enriched and the chromatin at *E(spl)-C* enhancers is accessible in the absence of Mam (Figure 7). These properties also persist for several hours after withdrawal of Notch activity and in this way, enhancers that have been switched on by Notch retain an imprint that can influence their response to a subsequent signal, a phenomenon known as transcriptional memory[76,77]. As an indication, after a previous Notch activation event, the conversion to an activation hub with Mam enrichment occurs more rapidly than in the absence of a prior active state. Similar accelerated recruitment of STAT1 to promoters occurred in cells with IFNγ-induced transcriptional memory [78], and augmented transcription levels have been seen in several contexts [79,80].

The concept that enhancers retain a memory of a recent Notch signal has several implications. First, naïve and pre-activated loci will respond with different kinetics, which could bias cell-fate decisions when iterative Notch signals are deployed [81]. Second, although our analysis has focussed on relatively short time scales (up to 8 hours), the footprint may be inherited by daughter cells as CSL is retained on mitotic chromosomes in at least some cell-types [82]. If this is the case, it may explain why enhancer decommissioning is important to switch-off the Notch response in some contexts [83–85]. Third, it could explain some of the observed recruitment of CSL corepressor complexes to active chromatin if they are involved in sustaining the hub when the signal decays [86,87].

Transcription initiation is probabilistic

Because the *in vivo* live imaging enables us to monitor the responses of individual nuclei, we made the surprising discovery that the presence of Mam-containing hubs at *E(spl)-C* is not sufficient to guarantee transcription. Instead, our results reveal that Mam recruitment confers a 1 in 3 chance of transcription. At any one time, only a third of nuclei are actively transcribing. This has profound implications because it has widely been assumed that stochastic differences in Notch pathway output arise due to

fluctuations in ligands or ligand availability [88,89] . Our results raise the possibility that differences may also arise due to intrinsic variations downstream of receptor activation that affect the probability of transcription occurring. Furthermore, this probability can be modified by other signals, as we observed here with ecdysone, or by the presence of other transcription factors, as when enhancers are 'primed' [90] and/or cooperatively regulated [91–95] .

In our experiments, the probability of transcription correlated with the proportion of nuclei where Med1, a core Mediator subunit, was recruited into the hub at *E(spl)-C*. Mediator is an important intermediary between transcription factors and the preinitiation complex and it functions as an 'integrator' coordinating diverse and combinatorial inputs [68]. The increased probability of Mediator recruitment can thus be explained by an increase in the valency of possible interactions when Notch and ecdysone are both active and present at the enhancers of target genes. We propose that this will be a general mechanism and that other signals/transcription factors will synergise with Notch complexes by adding to the valency of interactions and facilitating recruitment of coactivators to increase the probability of transcription. In different contexts this could toggle the response from one that is stochastic to one that is hard-wired.

Acknowledgements

We thank Kat Millen and the Genetics Department Fly Facility for performing DNA injections of fly embryos to generate transgenic stocks. We are grateful to Cambridge Advanced Imaging Centre for advice on imaging and to all members of the Bray Lab, for helpful discussions and comments on the manuscript. The work was funded by a Wellcome Trust Investigator Award (212207/Z/18) and an MRC Programme Grant (MR/T014156/1) to SJB. CR and SB were supported by studentships from Wolfson College-University of Cambridge (Dept of Physiology Development and Neuroscience-School of Biological Sciences)

Author contributions

JdeHA, MGL and SJB designed the experiments. JdeHA, SB, JMT performed the experiments. MGL generated critical reagents. JdeHA, CR, SB, JMT and SJB analysed the data. JdeHA and SJB wrote the manuscript, JdeHA, CR, SB, JMT MGL reviewed and commented on the manuscript.

Declaration of interests

The authors declare no competing interests.

Figure Legends

Figure 1: Enrichment and dynamics of Mastermind at *E(spl)-C*.

(A) Schematic overview of live imaging system used. *Drosophila* salivary glands have large nuclei with polytene chromosomes that facilitate imaging. *E(spl)-C* locus is labelled using Int (orange)/ParB (red) system. Activation complexes, [CSL (green), NICD (purple) and Mastermind (magenta)] and co-repression complexes [CSL and Hairless (brown)] are depicted.

(B) Live-imaging of GFP::Mam and GFP::CSL as indicated in relation to *E(spl)-C* marked by Int-ParB (magenta) in nuclei from Notch-OFF (*1151Gal4; UAS-LacZ*) and Notch-ON (*1151Gal4; UAS-NΔECD*) salivary glands. CSL and Mam are enriched at *E(spl)-C* in Notch-ON but not Notch-OFF cells. Average enrichment: each pixel represents average enrichment of all aligned images, centred on *E(spl)-C* locus. Enrichment profile: mean enrichment, with SEM, plotted on x-axis relative to position, y axis , centred on *E(spl)-C* (0). Grey area indicates region used for max enrichment. Max enrichment: mean of 10 pixels centred on *E(spl)-C* (Figure S1A) (Mam OFF, n=32, Mam OFF, n = 30; CSL OFF, n = 45, CSL ON, n = 28, for p-values see Table S3). Box encompasses range between 0.25 and 0.75 quantile, whiskers extend to furthest points not considered outliers, bar marks median, cross marks mean and each dot is the value for one nucleus. Scale bars represent 5um.

(C) Dynamics of CSL::GFP (green), GFP::Mam (magenta) and Hairless::GFP (brown) at *E(spl)-C* in Notch-ON cells measured by FRAP. Dots indicate 50% recovery. Legend summarizes numbers of nuclei (n) and time to 50% recovery (t1/2). Error represents the standard error of the mean (SEM). (**C'**) FRAP analysis of CSL and Mam in cells depleted for Hairless (*1151Gal4; UAS-Hairless RNAi*) controls from C are included for comparison.

(D) Trajectory density at *E(spl)-C* relative to whole nucleus from SPT of CSL::Halo (green) and Halo::Mam (pink) in Notch-OFF and Notch-ON cells. Both CSL and Mam are significantly enriched in Notch-ON. Box plots as in (B). CSL-OFF , n = 5, CSL-OFF, n = 7; Mam-OFF , n = 5, Mam-ON, n = 13; for p-values see Table S3.

(E, E') Survival curves depicting duration of trajectories in SPT of the indicated Halo fusion proteins in whole nuclei (E) and at *E(spl)-C* (E'), in Notch-ON cells. Whole nuclei

Figure 1

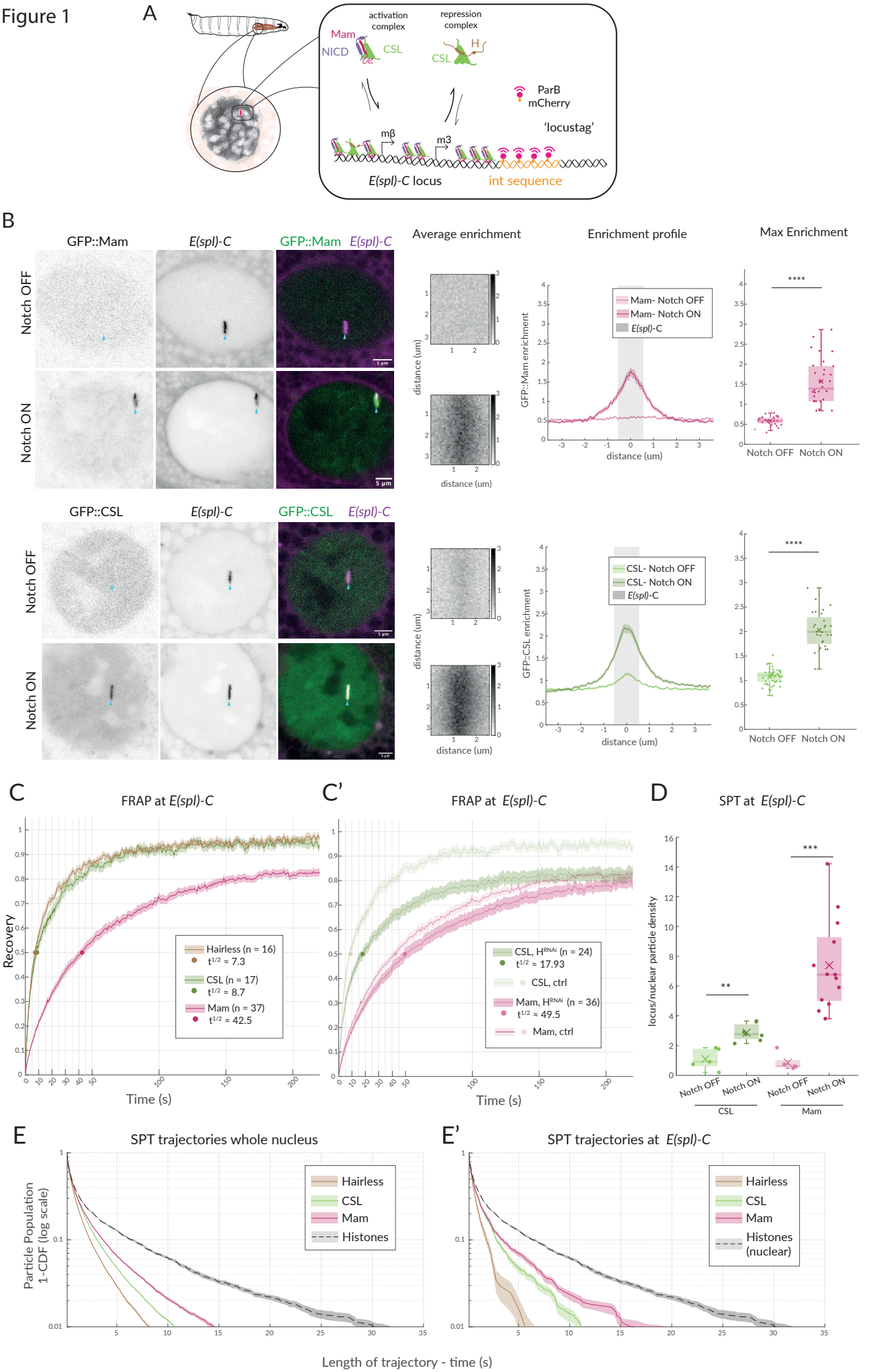
A
activation complex
repression complex
Mam
NICD
CSL
CSL
H
ParB mCherry
'locustag'
mβ
m3
E(spl)-C locus
int sequence
B
GFP::Mam
E(spl)-C
GFP::Mam E(spl)-C
Notch OFF
Notch ON
Average enrichment
Enrichment profile
Max Enrichment
distance (um)
GFP::Mam enrichment
Mam- Notch OFF
Mam- Notch ON
E(spl)-C
****
Notch OFF
Notch ON
GFP::CSL
E(spl)-C
GFP::CSL E(spl)-C
GFP::CSL enrichment
CSL- Notch OFF
CSL- Notch ON
C
FRAP at E(spl)-C
Recovery
Time (s)
Hairless (n = 16)
t1/2 ≈ 7.3
CSL (n = 17)
t1/2 ≈ 8.7
Mam (n = 37)
t1/2 ≈ 42.5
C'
FRAP at E(spl)-C
CSL, HRNAi (n = 24)
t1/2 ≈ 17.93
CSL, ctrl
Mam, HRNAi (n = 36)
t1/2 ≈ 49.5
Mam, ctrl
D
SPT at E(spl)-C
locus/nuclear particle density
**
***
CSL
Mam
E
SPT trajectories whole nucleus
Particle Population 1-CDF (log scale)
Hairless
CSL
Mam
Histones
E'
SPT trajectories at E(spl)-C
Histones (nuclear)
Length of trajectory - time (s)

H2B::Halo trajectories are included for comparison in both graphs. For number of trajectories, see Figure S1D. Error bars represent 95% confidence intervals, obtained from bootstrapping with 100 resampled datasets [96].
See also Supplementary Figure S1.

Figure 2: Hub-like properties of recruited complexes in Notch-ON nuclei.

(A) Representative images of GFP::CSL in Notch-ON nuclei containing an ectopic array of 12 or 48 CSL binding sites. GFP::CSL is recruited to *E(spl)-C* (yellow) and the ectopic array (blue). Average enrichment, Enrichment profile as in Figure 1B; (ectopic array 12, n=45, ectopic array 48, n = 40; *E(spl)-C* 12, n=45, *E(spl)-C* 48, n=40).

(B) Domain organisation of the indicated proteins are diagrammed above the prediction scores (IUPRED) of protein disorder for each. Regions tested as IDRs are indicated.

(C) Average enrichments and enrichment profiles of NICD-PEST IDR (Notch-OFF, n = 62, Notch-ON, n = 67) and CSL-nt IDR (Wilcoxon rank sum test: Notch-OFF, n = 8, Notch-ON, n = 40) at *E(spl)-C* in Notch-OFF and Notch-ON cells.

(D) Average enrichments and enrichment profiles (as in Figure 1B) of GFP::Mam at *E(spl)-C* in nuclei expressing intact (Nact) and IDR deleted (Nact ΔIDR) Notch constructs (Nact , n = 58, Nact ΔIDR, n = 55). p-values in Table T3

(E) Diagram illustrates concentric ring analysis of single particle trajectories at increasing distances from *E(spl)-C*. Graphs plot proportions of bound (dark shading) and diffusive (light shading) particles of Halo::Mam or Halo::CSL within each ring. Dashed lines indicate nuclear proportions of each population as indicated.

See also Supplementary Figure S2

Figure 3: Mam enrichment requires Mediator CDK module but is independent of transcription and CBP/p300.

(A-B) GFP::Mam recruitment levels and dynamics at *E(spl)-C* in Notch-ON tissues treated with triptolide or DMSO as a control. (A) Average and Max enrichment as in Figure 1B, (DMSO n = 49, triptolide, n = 36). (B) FRAP recovery curves, plotted as in Figure 1C.

(C–F) Average enrichment and Max enrichment of GFP::Mam and GFP::CSL, as indicated, at *E(spl)-C* in Notch-ON control and treated tissues**. (C-D)** No change in

Figure 2

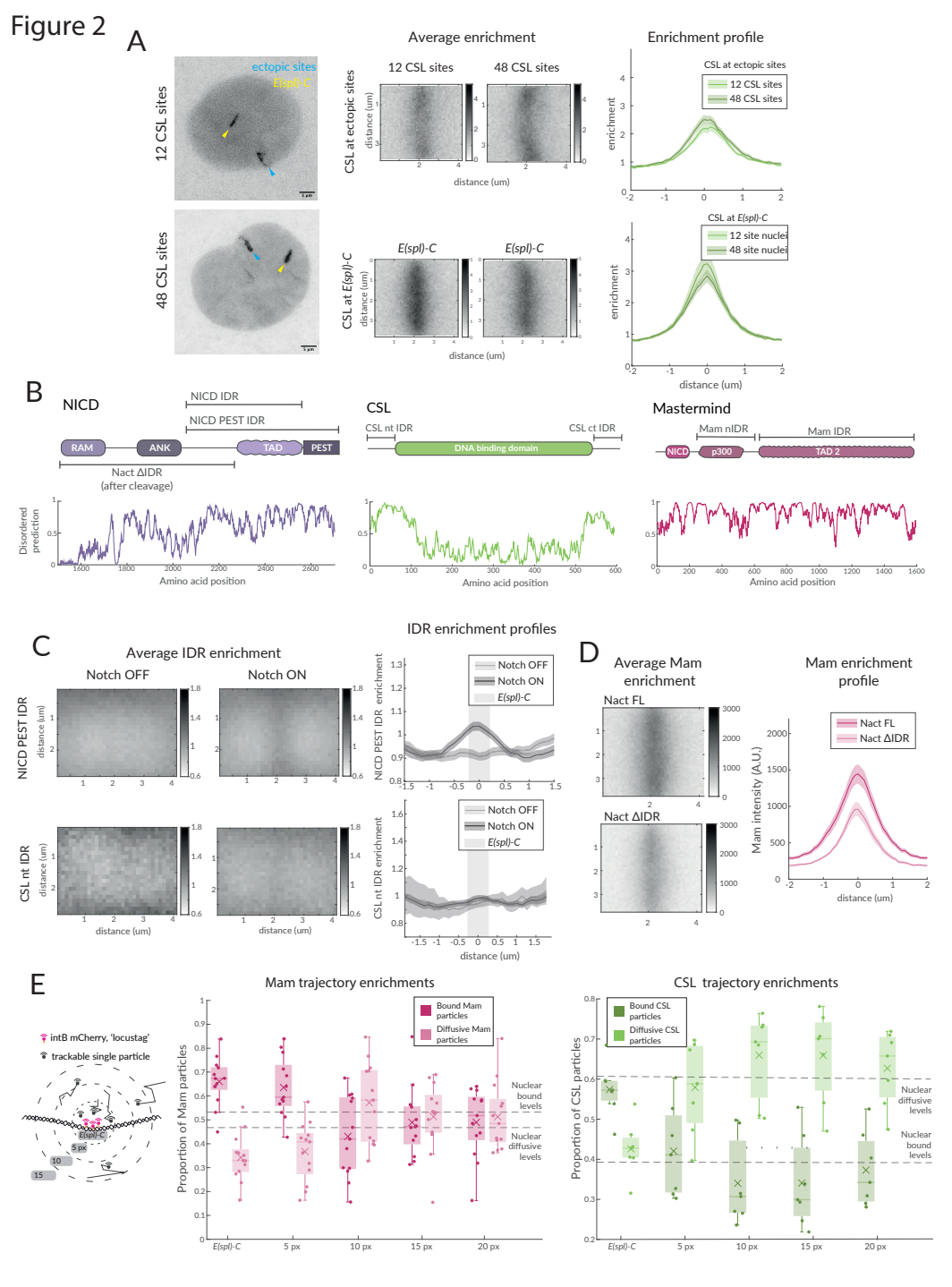
A
12 CSL sites
48 CSL sites
ectopic sites
E(spl)-C
Average enrichment
12 CSL sites
48 CSL sites
CSL at ectopic sites
CSL at E(spl)-C
distance (um)
Enrichment profile
CSL at ectopic sites
12 CSL sites
48 CSL sites
CSL at E(spl)-C
12 site nuclei
48 site nuclei
enrichment
B
NICD
NICD IDR
NICD PEST IDR
RAM
ANK
TAD
PEST
Nact ΔIDR
(after cleavage)
CSL
CSL nt IDR
CSL ct IDR
DNA binding domain
Mastermind
Mam nIDR
Mam IDR
NICD
p300
TAD 2
Disordered prediction
Amino acid position
C
Average IDR enrichment
Notch OFF
Notch ON
NICD PEST IDR
CSL nt IDR
distance (um)
IDR enrichment profiles
Notch OFF
Notch ON
E(spl)-C
NICD PEST IDR enrichment
CSL nt IDR enrichment
D
Average Mam enrichment
Nact FL
Nact ΔIDR
Mam enrichment profile
Nact FL
Nact ΔIDR
Mam intensity (A.U.)
distance (um)
E
intB mCherry, 'locustag'
trackable single particle
E(spl)-C
5 px
10
15
Mam trajectory enrichments
Bound Mam particles
Diffusive Mam particles
Proportion of Mam particles
Nuclear bound levels
Nuclear diffusive levels
E(spl)-C
5 px
10 px
15 px
20 px
CSL trajectory enrichments
Bound CSL particles
Diffusive CSL particles
Proportion of CSL particles
Nuclear diffusive levels
Nuclear bound levels

Figure 3

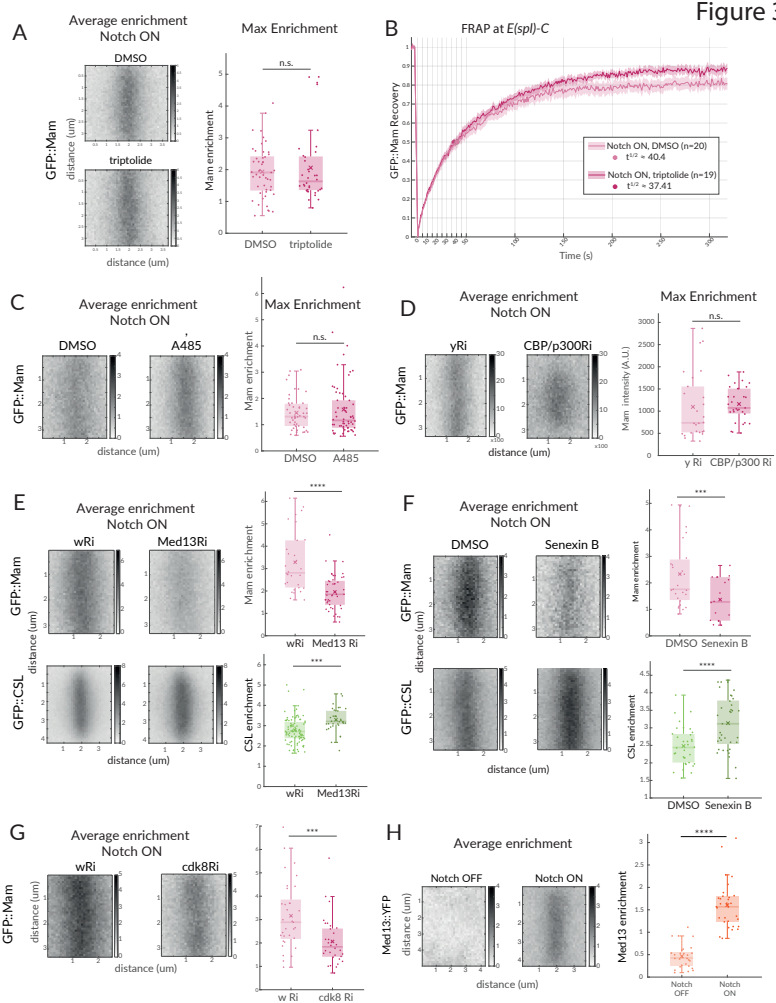
A
Average enrichment
Notch ON
DMSO
triptolide
GFP::Mam
distance (um)
Max Enrichment
n.s.
Mam enrichment
DMSO
triptolide
B
FRAP at E(spl)-C
GFP::Mam Recovery
Notch ON, DMSO (n=20)
t1/2 = 40.4
Notch ON, triptolide (n=19)
t1/2 = 37.41
Time (s)
C
Average enrichment
Notch ON
DMSO
A485
GFP::Mam
distance (um)
Max Enrichment
n.s.
Mam enrichment
DMSO
A485
D
Average enrichment
Notch ON
yRi
CBP/p300Ri
GFP::Mam
distance (um)
Max Enrichment
n.s.
Mam intensity (A.U.)
y Ri
CBP/p300 Ri
E
Average enrichment
Notch ON
wRi
Med13Ri
GFP::Mam
GFP::CSL
distance (um)
Mam enrichment
CSL enrichment
****
***
wRi
Med13 Ri
F
Average enrichment
Notch ON
DMSO
Senexin B
GFP::Mam
GFP::CSL
distance (um)
Mam enrichment
CSL enrichment
***
****
DMSO
Senexin B
G
Average enrichment
Notch ON
wRi
cdk8Ri
GFP::Mam
distance (um)
***
w Ri
cdk8 Ri
H
Average enrichment
Notch OFF
Notch ON
Med13::YFP
distance (um)
Med13 enrichment
****
Notch OFF
Notch ON

recruitment following inhibition (C, A485) or genetic knockdown (D, RNAi) of CBP/p300 compared to control, DMSO and yellow RNAi (yRi) respectively. (DMSO, n = 47, A485, n = 62; yRNAi, n = 26, CBP/p300 RNAi, n = 31). **(E, F)** Reduced recruitment of GFP::Mam (magenta) but not CSL::GFP (green) following (E) genetic knockdown of Med13 and (F) inhibition of CDK8 with Senexin B. (E: Mam control, n = 30 , Mam Med13Ri, n = 45; CSL control, n=92, CSL Med13Ri, n = 36) and (F: Mam ctrl n = 27, Mam Senexin, n = 43; CSL ctrl, n = 34, CSL Senexin, n = 37).

(G) Genetic knockdown of Cdk8 results in decreased Mam recruitment compared to controls (ctrl, n=33, Cdk8 Ri, n = 32). Box plots in A-F as in Figure 1B. For p-values see Table S3.

(H) Average enrichment and max enrichment of Med13::YFP at *E(spl)-C* in Notch-OFF, n = 28 and Notch-ON, n = 31; for p-values see Table S3.

See also Supplementary Figure S3.

Figure 4: Mam is not necessary for CSL enrichment and chromatin opening but necessary for transcription and Mediator 13 enrichment.

(A) Recruitment of GFP::Mam in Notch-ON nuclei is perturbed by MamDN (*1151-Gal4 UAS-MamDN*) (A) while recruitment of GFP::CSL is unaffected (A'). Control UAS were included in Notch-ON combinations, details are provided in Table S4. Scale bars represent 5um.

(B) Accessibility of Notch regulated enhancers adjacent to *E(spl)bHLH*-mβ and *E(spl)bHLH*-m3 under the conditions indicated was probed using ATAC-qPCR. Values were normalised to Rab11, error bars represent SEM. Closed control is a noncoding genomic region in chromosome 3 and open control' Eip78, an ecdysone responsive region active in L3 larval stage.

(C) Average enrichment and max enrichment of Med13::YFP at *E(spl)-C* in Notch-ON conditions only, and in combination with MamDN. Quantifications as in Figure 1B, OFF, n=28, ON, n = 31. For p-values see Table S3

(D-D') Expression of *E(spl)bHLH*-m3, detected by smFISH in the conditions indicated; representative images from cytoplasm (upper; 1.8mm^3) and nucleus (lower; centred on *E(spl)-C*, blue arrows). Scale bars represent 5um. Graphs (D'), number of RNA puncta (cytoplasmic, n = 18, 20 and 22) and locus intensity (nucleus, n = 6, 7 and 6) in Notch

Figure 4

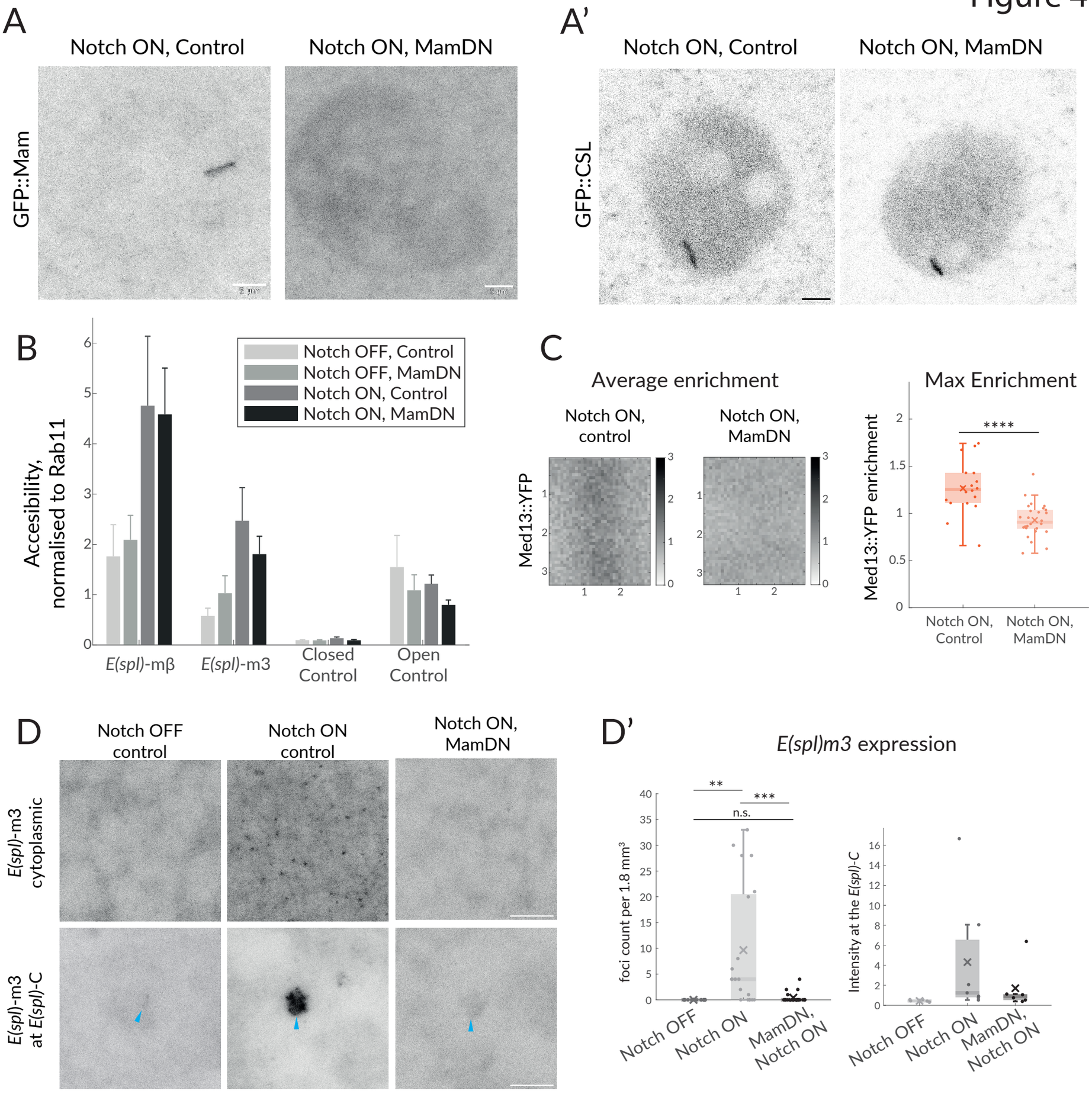
A
Notch ON, Control
Notch ON, MamDN
GFP::Mam
A'
Notch ON, Control
Notch ON, MamDN
GFP::CSL
B
Notch OFF, Control
Notch OFF, MamDN
Notch ON, Control
Notch ON, MamDN
Accesibility, normalised to Rab11
E(spl)-mβ
E(spl)-m3
Closed Control
Open Control
C
Average enrichment
Notch ON, control
Notch ON, MamDN
Med13::YFP
Max Enrichment
Med13::YFP enrichment
****
Notch ON, Control
Notch ON, MamDN
D
Notch OFF control
Notch ON control
Notch ON, MamDN
E(spl)-m3 cytoplasmic
E(spl)-m3 at E(spl)-C
D'
E(spl)m3 expression
foci count per 1.8 mm³
**
***
n.s.
Notch OFF
Notch ON
MamDN, Notch ON
Intensity at the E(spl)-C

OFF, Notch ON ctrl and Notch ON MamDN as indicated, boxplots as described in Figure 1B.

See also Supplementary Figure S4.

Figure 5: Effects of Notch withdrawal on hub composition imply memory state.

(A) Temperature paradigm: Withdrawal of Notch activity using the thermosensitive Gal4/Gal80ts system; after a 24h ON period, larvae were transferred to non-permissive temperatures for the indicated periods (top) and enrichment of mCherry::CSL and GFP::Mam at *E(spl)-C* imaged. Average enrichment, enrichment profiles and max enrichment quantified as in Figure 1B. 24 hrs ON, n = 28, 24 hrs ON, 4 hrs OFF, n = 21, 24 hrs ON, 8 hrs OFF, n = 19. p-values are summarized in Table S3.

(B) Accessibility of enhancers at *E(spl)bHLH*-mβ and *E(spl)bHLH*-m3, in Notch-ON and after Notch withdrawal (8 hours) was probed using ATAC-qPCR, as in Figure 4B.

(C) Expression of *E(spl)bHLH*-m3, detected by smFISH in the conditions indicated; representative images from cytoplasm (upper; 1.8 mm^3) and nucleus (lower; centred on *E(spl)-C*, *blue* arrow). Representative images are shown, scale bars represent 5um. Graphs show number of RNA puncta (cytoplasmic) from n = 22, 30 and 30 regions, with boxplots as described before (Figure 1B). p-values in Table S3.

(D) Optogenetic paradigm: Conditions used to switch ON and OFF Notch activity using OptiC Notch [67].

(E) Recruitment of CSL::GFP and Mam::Halo at *E(spl)-C*, measured following blue light activation for 2 hours (ON) and after 4 hours in dark (OFF). GFP::CSL remains enriched, Halo::Mam is depleted.

(F) Recruitment of Halo::Mam in preactivated nuclei compared to naïve nuclei; temporal profile of Mam::Halo enrichment (right) and time taken to max enrichment (left). Error bars in the profile represents the SEM, values were normalised from 0 to 1 (similar to FRAP recovery, see Figure 1 and methods), n indicates the number of nuclei from >3 salivary glands. Boxplots parameters as in Figure 1B; naïve, n = 11, preactivated n = 9.

Figure 5

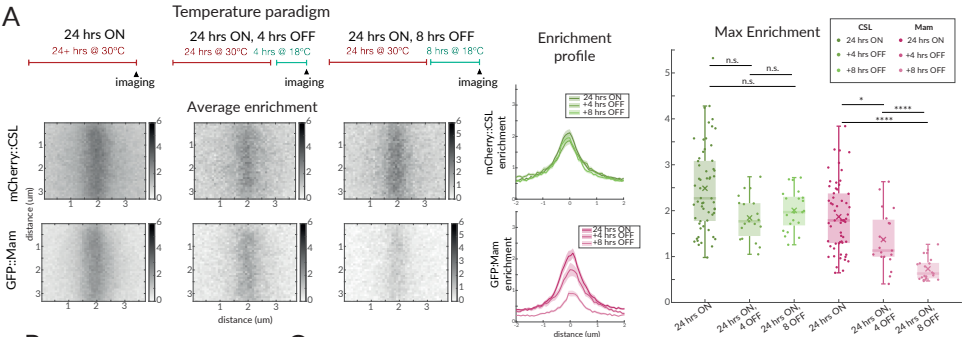
A
Temperature paradigm
24 hrs ON
24+ hrs @ 30°C
imaging
24 hrs ON, 4 hrs OFF
24 hrs @ 30°C
4 hrs @ 18°C
imaging
24 hrs ON, 8 hrs OFF
24 hrs @ 30°C
8 hrs @ 18°C
imaging
Average enrichment
mCherry::CSL
GFP::Mam
distance (um)
Enrichment profile
24 hrs ON
+4 hrs OFF
+8 hrs OFF
mCherry::CSL enrichment
GFP::Mam enrichment
Max Enrichment
CSL
Mam
24 hrs ON
+4 hrs OFF
+8 hrs OFF
n.s.
*
****

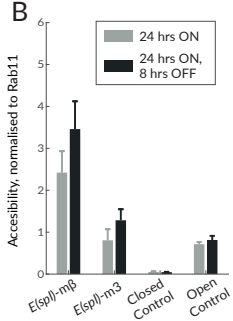
B
24 hrs ON
24 hrs ON, 8 hrs OFF
Accesibility, normalised to Rab11
E(spl)-mβ
E(spl)-m3
Closed Control
Open Control

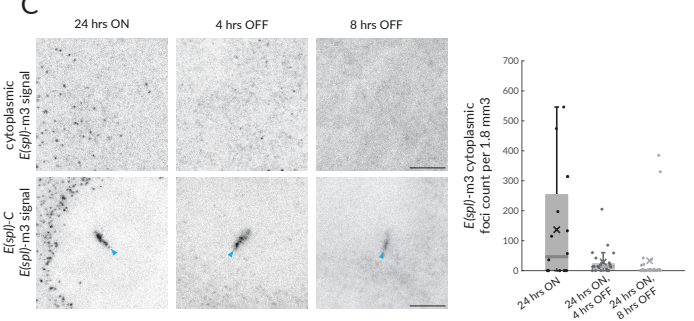
C
24 hrs ON
4 hrs OFF
8 hrs OFF
cytoplasmic E(spl)-m3 signal
E(spl)-C E(spl)-m3 signal
E(spl)-m3 cytoplasmic foci count per 1.8 mm3
24 hrs ON
24 hrs ON, 4 hrs OFF
24 hrs ON, 8 hrs OFF

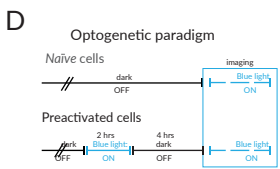
D
Optogenetic paradigm
Naïve cells
dark
OFF
imaging
Blue light
ON
Preactivated cells
dark
OFF
2 hrs
Blue light
ON
4 hrs
dark
OFF
Blue light
ON

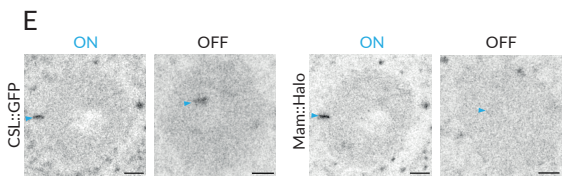
E
ON
OFF
CSL::GFP
ON
OFF
Mam::Halo

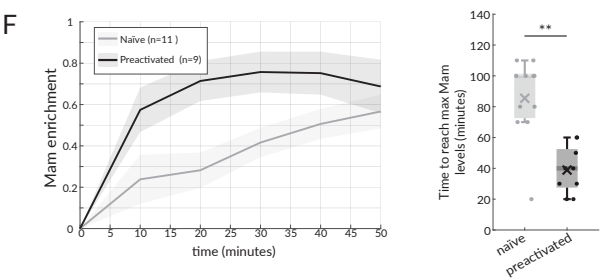
F
Naïve (n=11)
Preactivated (n=9)
Mam enrichment
time (minutes)
Time to reach max Mam levels (minutes)
**
naïve
preactivated

Figure 6: Recruitment of Pol II and Med1 in Notch-ON is infrequent and is augmented by ecdysone.

(A) GFP::Mam enrichment at *E(spl)-C* in Notch-OFF and Notch-ON conditions as in Figure 1, represented with a violin plot with mean marked by a cross and median by a bar. Right graph: proportions of nuclei with significant enrichment (obtained by performing a Gaussian fit on the fluorescence intensity Images, see Supplementary Figure S5). Over 90% nuclei have significant enrichment (Notch-OFF, n = 32, Notch-ON, n = 30)

(B) Recruitment of GFP::Rbp1, a subunit of Pol II, at *E(spl)-C* in Notch-OFF and Notch-ON nuclei. Images: example where enrichment is detected. Graph: proportions of nuclei with significant enrichment as in A (Notch-OFF, n = 37, Notch-ON, n = 43). All scale bars represent 5um.

(C) Recruitment of GFP::Med1 at *E(spl)-C* in Notch-OFF and Notch-ON nuclei. Images: example where enrichment is detected. Graph: proportions of nuclei with significant enrichment as in A (Notch-OFF and ON, n = 38, 62). All scale bars represent 5um.

(D) Transcriptional activity in Notch-ON cells detected using live imaging of GFP::MCP recruited to MS2 loops in transcripts produced by *E(spl)bHLH*mβ (see methods). Images: representative examples of active (upper) and inactive (lower) nuclei. Graph: Proportion of active nuclei (Notch-ON, n = 53)

(E) Recruitment of GFP::Med1, mCherry::Rbp1 and Halo::CSL. Med1 and Rbp1 recruitments are correlated. Images: example of co-recruitment of Med1, Rbp1 and CSL. Graph: Correlation plot of max enrichment per nucleus at *E(spl)-C*, (marked by Halo::CSL recruitment), n = 48.

(F) Pretreatment with ecdysone in Notch-ON conditions increases proportions of nuclei with recruitment of GFP::Rbp1, GFP::Med1 and with active transcription foci (MS2/MCP intensity) compared to controls (ETOH). Proportions of nuclei with significant enrichment defined as in A. Rbp3 ctrl, ecdysone: n = 39, 36. Med1 ctrl, ecdysone: n = 34, 34. MS2 ON ctrl, ON ecdysone, OFF ecdysone: n = 52, 42, 22.

See also Supplementary Figure S5.

Figure 6

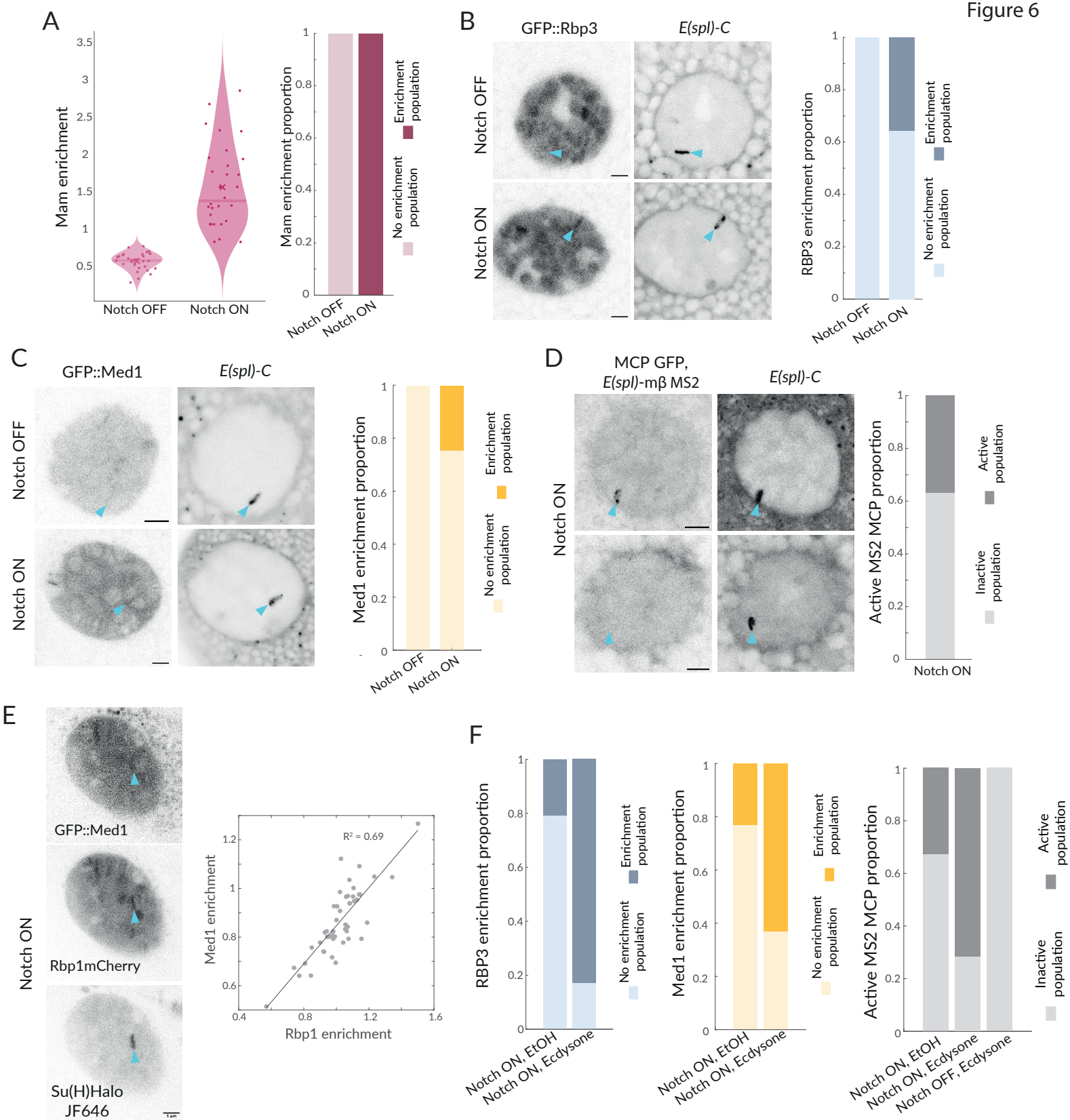
A
Mam enrichment
Notch OFF
Notch ON
Mam enrichment proportion
Enrichment population
No enrichment population
B
GFP::Rbp3
E(spl)-C
Notch OFF
Notch ON
RBP3 enrichment proportion
C
GFP::Med1
Med1 enrichment proportion
D
MCP GFP, E(spl)-mβ MS2
Active MS2 MCP proportion
Active population
Inactive population
E
GFP::Med1
Rbp1mCherry
Su(H)Halo JF646
R² = 0.69
Med1 enrichment
Rbp1 enrichment
F
Notch ON, EtOH
Notch ON, Ecdysone
Notch OFF, Ecdysone

Figure 7. Model illustrating different modes of Notch transcription-hub.

In the absence of Notch activity (Notch-OFF) target genes are inactive, CSL is complexed with co-repressors (e.g. Hairless). Following Notch activation (Notch ON), released NICD (purple) generates a localized high concentration of transcription factors around target enhancer(s) referred to as a "hub" (orange). Open hub: CSL (green) recruitment and accessible chromatin can occur in the absence of Mam. Engaged hub: presence of Mam (magenta) favours recruitment of additional factors, including Mediator CDK8 module (yellow). Active hub: productive transcription, transition to this mode, with core Mediator (yellow) and Pol II (pale blue) enrichment, is stochastic (dotted arrow). The probability can be enhanced by secondary signal, such as provided by ecdysone. Memory hub: CSL enrichment and chromatin accessibility remain after withdrawal of NICD.

Figure 7

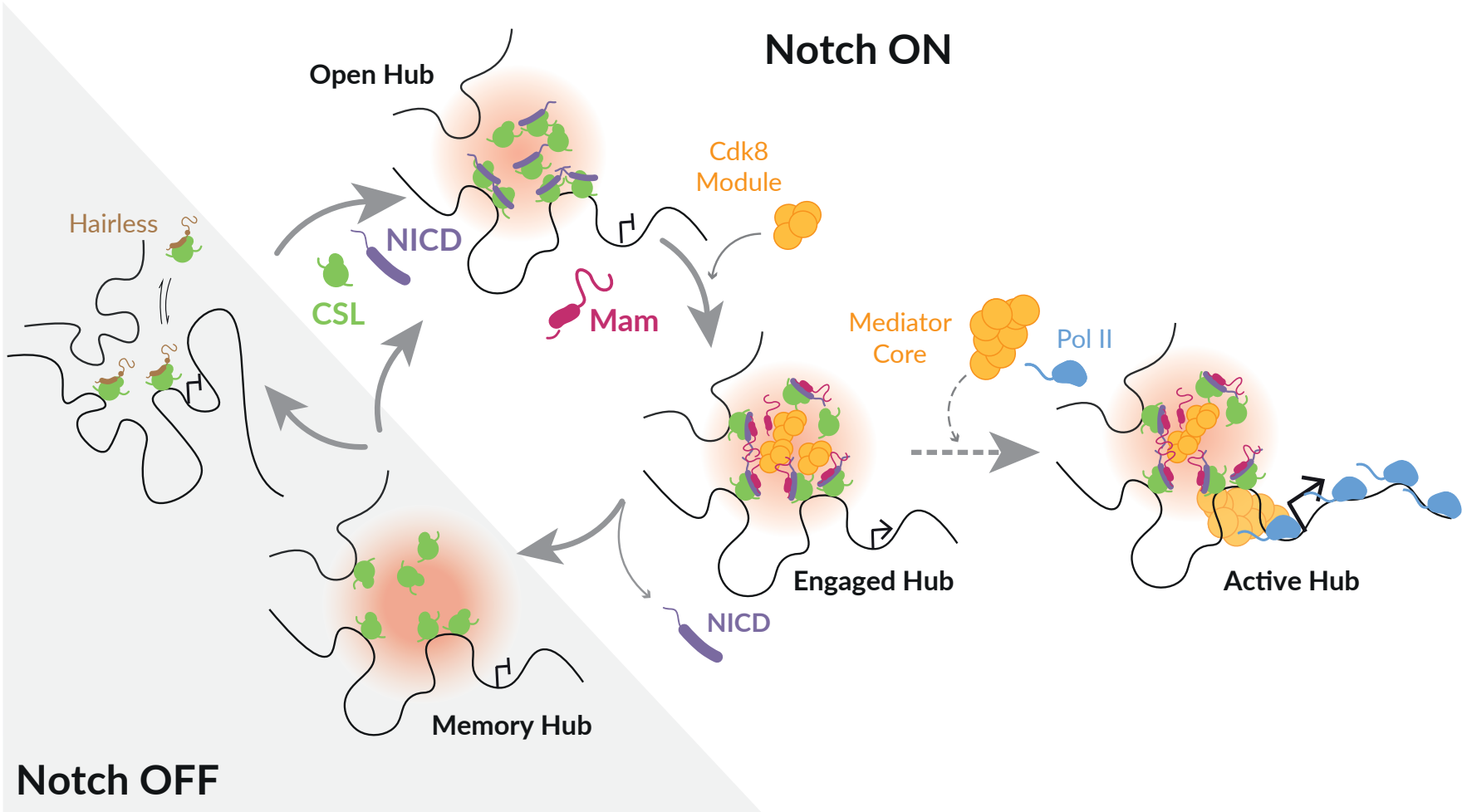
Notch ON
Open Hub
Cdk8
Module
Hairless
NICD
CSL
Mam
Mediator
Core
Pol II
Engaged Hub
Active Hub
NICD
Memory Hub
Notch OFF

STAR Methods

Experimental Animals

Species: *Drosophila melanogaster*. Flies were grown and maintained on food consisting of the following ingredients: Glucose 76g/l, Cornmeal flour 69g/l, Yeast 15g/l, Agar 4.5g/l, Methylparaben 2.5ml/l. Animals of both sexes were used for this study.

Fly Stocks

For genetic manipulations of Notch activity, the Gal4 driver line *1151-Gal4* was combined with *UAS-NΔECD* to provide constitutively active Notch [37,38] or with *UAS-LacZ* as a control. In experiments with fluorescent labelled proteins the following were used: GFP::CSL and GFP::Hairless[34], Halo::CSL, Med13::YFP (BL-57899). Experiments measuring in vivo recruitment to *E(spl)-C* utilized a "locus tag" chromosome in which Int1 sequences had been inserted into an *E(spl)-C* intergenic region and recombined with *UAS-ParB1-mcherry* or *UAS-ParB1-GFP* inserted *AttP.86Fb* [34]

To manipulate protein functions, RNAi lines were as listed in Table S2 and included UAS-Hairless-RNAi (Bloomington Drosophila Stock Center, BL-27315), UAS-Mam-RNAi (BL-28046), UAS-Med13-RNAi (BL-34630), UAS-nejire-RNAi (Vienna Drosophila Resource Center, VDRC-102885), UAS-Cdk8-RNAi (gifted by [97]) or with UAS-MamDN to block Mam activity [65]. Controls appropriate for each chromosome were UAS-yellow- RNAi (II), UAS-white-RNAi (III). Crosses were maintained at 25°C.

For temperature manipulations *MS1096-Gal4* (BL-8860) was recombined with *tubulin-Gal80ts* and flies were switched between 29°C permissive and 18°C non-permissive temperatures.

For photomanipulation, transgenes *UAS-Cry2-TevC* and *UAS-OptICNotch{ω}* were recombined onto one chromosome and the conditions used were as described [67].

For MCP/MS2 live imaging of transcription, a strain in which 24M2 loops were inserted into *E(spl)*mβ-HLH gene was generated by CRISPR using the strategy described [11] details are provided in Table T2. This was combined with *hsp83-MCP::GFP* (BL-7280).

Generation of tagged Mastermind and Med1 flies:

CRISPR/cas9 genome engineering was used to introduce fluorescent (sfGFP) or Halo tags into N-terminal coding regions of Mam and Med1 (flycrispr.org) to generate seamless protein fusions. Briefly, plasmids for expression of the gRNA (pCFD3-dU6) and for homology arm

repair (pHD-ScarlessDsRED) were injected into *nanos-cas9* flies (flycrispr.org). Transformants were selected based on the expression of 3xPax3-dsRED which was subsequently removed by crossing to *αTub84B-PiggyBac* flies (BL-32070). Details of gRNA and homology sequences are provided in Table S1.

Generation of flies expressing IDR-GFP fusions

IDR regions of CSL, NICD, Med1 and Mam were isolated from genomic DNA by PCR (Table S1) and inserted into the plasmid pUASt-attB (DGRC, 1419). sfGFP was inserted into the N terminus so that the coding sequences generated an in-frame protein fusion. The resulting plasmids contained an attB sequence and were injected into a strain containing phiC31 integrase and AttP site in position *AttP40* (chromosome II, BL-25709) to obtain transgenic flies for conditional expression of the IDR fusions.

Method Details

Salivary Gland culture and drug/hormonal treatments

Salivary glands were dissected and mounted as described in [34], by submerging mid L3 larvae in M3 Shields and Sang media (Sigma-Aldrich, S3652) supplemented with 5% fetal bovine serum (Sigma-Aldrich, F9665) and 1× Antibiotic-Antimycotic (Gibco,15240-062). For drug and hormonal treatments dissected glands were incubated for an hour with the following compounds: triptolide (10uM, Sigma-Aldrich T3652), Ecdysone (5uM, Cayman Chemicals 16145), A485 (5uM, Cayman Chemicals 24119), Senexin A (1uM, Tocris 4875) and Senexin B (2uM, Cayman Chemicals 24119). After dissection and any treatments glands were mounted into PolyLysine coated coverslips in dissection media supplemented with methyl-cellulose (Sigma-Aldrich, M0387-100G).

Confocal Imaging and FRAP analysis

Live confocal fluorescence imaging of salivary glands was performed on a Leica SP8 microscope equipped with 7 laser lines (405, 458, 488, 496, 514, 561, and 633) and a 63×/1.4 NA HC PL APO CS2 oil immersion objective and two hybrid GaAsP detectors. Individual nuclei were imaged with a 4.5x zoom, 512×512 pixel resolution, pinhole set to 3-Airy, three line averages, a 12-bit depth and 600 Hz scanning speed. Z-stacks were chosen to encompass the locus and around 9 stacks were acquired. The step size was chosen based on pinhole aperture and was <1um. FRAP was performed on the same microscope but settings were optimised for

bleaching and scanning speed: pinhole was opened to 3.5-Airy, speed was increased to 700 Hz, line averaging was removed and Leica FRAP booster was activated. Effective bleaching was achieved by point bleaching. Images before and after bleaching were acquired every 0.4 seconds. After 50 images post bleaching, frame gap was increased to 1 second to minimise unintentional bleaching.

FRAP curves were normalised as described [34], by applying the following:

$$Recovery = \frac{T_{pre} \times B_t}{T_t \times B_{pre}}$$

Where intensities are *Tpre* in a nuclear region before bleaching, *Bt* in the bleached region throughout the experiment, *Tt* in a nuclear region throughout the experiment and *Bpre* the bleached region throughout the experiment.

Single Particle Imaging

Sample preparation and imaging for Single Particle Tracking (SPT) experiments was performed as in [42]**.** Briefly after dissection glands were incubated with Halo ligand, TMR (Promega, G825A) for 15min and washed fin 3 consecutive 10min baths of dissecting medium. Halo ligand concentrations used were 10nM, 10nM, 50nM and 0.01-0.02nM for CSL, Hairless, Mastermind and Histone H2AV respectively. Larvae were imaged on custom build inverted microscope optimised for Single Molecule Localisation Microscopy [34,42] with 50ms exposure time, for 3 to 7min approximately per nuclei.

Immunofluorescence and in situ hybridization

Salivary glands were prepared for immunofluorescence as described before [34]. Larvae were submerged in PBS and salivary glands were dissected and then fixed in 4% formaldehyde for 15 minutes. Glands were washed three times in PBS + 0.3% Triton X-100. They were later blocked by adding 1% BSA to this buffer. Primary antibody incubation was performed overnight at 4°C with αGFP (1/500, ThermoFisher A6455) and αRFP (1/1000, Chromotek 5F8), αH3K27ac (1/500, ActiveMotif 39135). Glands were washed at least three times with BSA containing buffer, followed by secondary antibody and nuclear stain incubation for two hours at RT (Jackson ImmunoResearch Laboratories, Inc and Sigma). Lastly, they were washed three times and mounted in Vectashield. Image acquisition was performed similarly to live imaging but with a with pinhole closed to 1 Airy and an optimised Z step size, a 0.75 zoom and a 1024x1024 px resolution.

smFISH probes were designed with Stellaris Probe tool for *E(spl)m3-HLH* and salivary glands were processed as described [11]. Briefly, glands were fixed for 45 minutes in 3.7% formaldehyde at RT and permeabilized with overnight in 70% EtOH at 4°C Hybridization and washes were performed according to manufacturer's instructions. Image acquisition was performed similarly to live imaging but with a with pinhole closed to 1 Airy and an optimised Z step size and a 10x zoom. Cytoplasmic images always contained constant Z steps.

ATAC qPCR

Accessibility of genomic regions was probed by tagmention reaction coupled with qPCR, as described [34]. Briefly, salivary glands were lysed and nuclei were suspended in TD buffer and TD DNA tagment enzyme was added (Illumina #FC-121- 1030). The chromatin was tagmented for minutes at 37°C . DNA was amplified with Nextera primers, and samples were normalised by running qPCRs and determining the necessary extra cycles for each sample. Standard qPCRs were performed to quantify accessibility of different regions (Roche #04707516001).

Analysis

Confocal image analysis

Images were analysed using MATLAB by importing Leica Images with BioFormat package (MATLAB R2022b, Mathworks & openmicroscopy.org). A custom MATLAB app was built to select and rotate the Z stack of interest. A rectangular region of interest of 90x40 pixels was selected for each nucleus. Additionally, three circular regions were drawn to measure the nuclear levels in the selected stack, which by division or subtraction enabled normalisation of the rectangular ROI. The ROIs obtained are centred, and this allowed averaging experimental conditions, referred to as "Averaged intensities or enrichment". For the profiles, the ROIs were averaged in the y dimension, and the mean and SEM were represented for each condition. Lastly, for the max enrichment the 10 middle pixels were obtained from the intensity or enrichment profile. To obtain proportions of enrichment cells, gaussian fitting of enrichment values was applied, where the proportion, mean and sigma were used to characterize the enrichment populations. In the correlation, R^2 is the proportion of variance of y explained by the variance of x calculated as 1-RSS/TSS; RSS = sum of squared residuals; TSS = total sum of squares.

SPT analysis

SMLM movies were analysed using the pipeline described in [42]. Localisation of single molecules was carried out using a Gaussian fitting-based approach [98] while a multiple hypothesis tracking algorithm based on [99] was used for tracking. No detection gaps were allowed in tracking except in the case of analyses focusing solely on the duration of trajectories (Figure 1E), for which up to 3 detection gaps were allowed. Trajectories consisting of at least 4 time points were then analysed with a Bayesian treatment of HMM, vbSPT [100] and assigned into 2 states, each defined by a Brownian motion diffusion coefficient.

Trajectory density analysis shown in Fig 1D was carried out by comparing near-locus density with nuclear density using the formula:

$$\frac{No.\,of\ trajectories\ near\ locus}{Total\ no.\,of\ trajectories\ in\ nucleus} \times \frac{Nucleus\ area}{Locus\ area}.$$

Locus and nucleus areas were calculated with standard MATLAB procedures, using the convex hull of localisations and masking.

1-CDF survival curves (Fig 1E) were plotted using 99% of trajectories for each molecule, excluding the longest 1% of trajectories which could be artifacts and would have therefore biased our data.

Statistical analysis

N numbers indicate number of nuclei images, unless stated otherwise. If n >30 for both conditions tested, a two tailed t-test was applied. Otherwise, normality was checked via a Shapiro-Wilk test. If both samples were not normal, a Wilcoxon rank sum test was applied. In all cases significance was presented as follows: * if $p < 0.05$, ** if $p < 0.01$, *** if $p < 0.001$ and **** if $p < 0.0001$ and p-values are provided in Table S3

References

1. Bray, S.J. (2016). Notch signalling in context. Nat Rev Mol Cell Biol *17*, 722–735. 10.1038/nrm.2016.94.
2. Kopan, R. (2012). Notch signaling. Cold Spring Harb Perspect Biol *4*. 10.1101/cshperspect.a011213.
3. Borggrefe, T., and Oswald, F. (2009). The Notch signaling pathway: Transcriptional regulation at Notch target genes. Cellular and Molecular Life Sciences *66*, 1631–1646. 10.1007/s00018-009-8668-7.
4. Kovall, R.A., Gebelein, B., Sprinzak, D., and Kopan, R. (2017). The Canonical Notch Signaling Pathway: Structural and Biochemical Insights into Shape, Sugar, and Force. Dev Cell *41*, 228–241. 10.1016/j.devcel.2017.04.001.
5. Kopan, R., and Ilagan, M.X.G. (2009). The Canonical Notch Signaling Pathway: Unfolding the Activation Mechanism. Cell *137*, 216–233. 10.1016/j.cell.2009.03.045.
6. Sprinzak, D., and Blacklow, S.C. (2021). Biophysics of Notch Signaling. Annu Rev Biophys *50*, 157–189. 10.1146/annurev-biophys-101920-082204.
7. Oswald, F., and Kovall, R.A. (2018). CSL-Associated Corepressor and Coactivator Complexes. In, pp. 279–295. 10.1007/978-3-319-89512-3_14.
8. Nam, Y., Sliz, P., Song, L., Aster, J.C., and Blacklow, S.C. (2006). Structural Basis for Cooperativity in Recruitment of MAML Coactivators to Notch Transcription Complexes. Cell *124*, 973–983. 10.1016/j.cell.2005.12.037.
9. Wilson, J.J., and Kovall, R.A. (2006). Crystal structure of the CSL-Notch-Mastermind Ternary complex bound to DNA. Cell *124*, 985–996. 10.1016/j.cell.2006.01.035.
10. Bray, S.J., and Gomez-Lamarca, M. (2018). Notch after cleavage. Curr Opin Cell Biol *51*, 103–109. 10.1016/j.ceb.2017.12.008.
11. Boukhatmi, H., Martins, T., Pillidge, Z., Kamenova, T., and Bray, S. (2020). Notch Mediates Inter-tissue Communication to Promote Tumorigenesis. Current Biology *30*, 1809-1820.e4. 10.1016/j.cub.2020.02.088.

12. Ilagan, M.X.G., Lim, S., Fulbright, M., Piwnica-Worms, D., and Kopan, R. (2011). Real-time imaging of Notch activation with a luciferase complementation-based reporter. Sci Signal *4*. 10.1126/scisignal.2001656.
13. Housden, B.E., Fu, A.Q., Krejci, A., Bernard, F., Fischer, B., Tavaré, S., Russell, S., and Bray, S.J. (2013). Transcriptional Dynamics Elicited by a Short Pulse of Notch Activation Involves Feed-Forward Regulation by E(spl)/Hes Genes. PLoS Genet *9*, e1003162. 10.1371/journal.pgen.1003162.
14. Cramer, P. (2019). Organization and regulation of gene transcription. Nature *573*, 45–54. 10.1038/s41586-019-1517-4.
15. Lee, T.I., and Young, R.A. (2013). Transcriptional Regulation and Its Misregulation in Disease. Cell *152*, 1237–1251. 10.1016/j.cell.2013.02.014.
16. Cho, C.Y., Kemp, J.P., Duronio, R.J., and O'Farrell, P.H. (2022). Coordinating transcription and replication to mitigate their conflicts in early Drosophila embryos. Cell Rep *41*, 111507. 10.1016/j.celrep.2022.111507.
17. Sabari, B.R., Dall'Agnese, A., Boija, A., Klein, I.A., Coffey, E.L., Shrinivas, K., Abraham, B.J., Hannett, N.M., Zamudio, A. V., Manteiga, J.C., et al. (2018). Coactivator condensation at super-enhancers links phase separation and gene control. Science *361*. 10.1126/science.aar3958.
18. Cho, W.-K., Spille, J.-H., Hecht, M., Lee, C., Li, C., Grube, V., and Cisse, I.I. (2018). Mediator and RNA polymerase II clusters associate in transcription-dependent condensates. Science *361*, 412–415. 10.1126/science.aar4199.
19. Rippe, K., and Papantonis, A. (2022). Functional organization of RNA polymerase II in nuclear subcompartments. Curr Opin Cell Biol *74*, 88–96. 10.1016/j.ceb.2022.01.005.
20. Brodsky, S., Jana, T., Mittelman, K., Chapal, M., Kumar, D.K., Carmi, M., and Barkai, N. (2020). Intrinsically Disordered Regions Direct Transcription Factor In Vivo Binding Specificity. Mol Cell *79*, 459-471.e4. 10.1016/j.molcel.2020.05.032.
21. Trojanowski, J., Frank, L., Rademacher, A., Mücke, N., Grigaitis, P., and Rippe, K. (2022). Transcription activation is enhanced by multivalent interactions independent of phase separation. Mol Cell *82*, 1878-1893.e10. 10.1016/j.molcel.2022.04.017.

22. Demmerle, J., Hao, S., and Cai, D. (2023). Transcriptional condensates and phase separation: condensing information across scales and mechanisms. Nucleus *14*. 10.1080/19491034.2023.2213551.
23. Hnisz, D., Shrinivas, K., Young, R.A., Chakraborty, A.K., and Sharp, P.A. (2017). A Phase Separation Model for Transcriptional Control. Cell *169*, 13–23. 10.1016/j.cell.2017.02.007.
24. Trylinski, M., Mazouni, K., and Schweisguth, F. (2017). Intra-lineage Fate Decisions Involve Activation of Notch Receptors Basal to the Midbody in Drosophila Sensory Organ Precursor Cells. Current Biology *27*, 2239-2247.e3. 10.1016/j.cub.2017.06.030.
25. Kitagawa, M. (2015). Notch signalling in the nucleus: roles of Mastermind-like (MAML) transcriptional coactivators. J Biochem, mvv123. 10.1093/jb/mvv123.
26. Just Ribeiro, M., and Wallberg, A. (2009). Transcriptional Mechanisms by the Coregulator MAML1. Curr Protein Pept Sci *10*, 570–576. 10.2174/138920309789630543.
27. Baghdadi, M.B., Castel, D., Machado, L., Fukada, S., Birk, D.E., Relaix, F., Tajbakhsh, S., and Mourikis, P. (2018). Reciprocal signalling by Notch–Collagen V–CALCR retains muscle stem cells in their niche. Nature *557*, 714–718. 10.1038/s41586-018-0144-9.
28. Castel, D., Mourikis, P., Bartels, S.J.J., Brinkman, A.B., Tajbakhsh, S., and Stunnenberg, H.G. (2013). Dynamic binding of RBPJ is determined by Notch signaling status. Genes Dev *27*, 1059–1071. 10.1101/gad.211912.112.
29. Rogers, J.M., Guo, B., Egan, E.D., Aster, J.C., Adelman, K., and Blacklow, S.C. (2020). MAML1-Dependent Notch-Responsive Genes Exhibit Differing Cofactor Requirements for Transcriptional Activation. Mol Cell Biol *40*. 10.1128/MCB.00014-20.
30. Fryer, C.J., Lamar, E., Turbachova, I., Kintner, C., and Jones, K.A. (2002). Mastermind mediates chromatin-specific transcription and turnover of the notch enhancer complex. Genes Dev *16*, 1397–1411. 10.1101/gad.991602.
31. Fryer, C.J., White, J.B., and Jones, K.A. (2004). Mastermind Recruits CycC:CDK8 to Phosphorylate the Notch ICD and Coordinate Activation with Turnover. Mol Cell *16*, 509–520. 10.1016/j.molcel.2004.10.014.

32. Janody, F., and Treisman, J.E. (2011). Requirements for mediator complex subunits distinguish three classes of notch target genes at the Drosophila wing margin. Developmental Dynamics *240*, 2051–2059. 10.1002/dvdy.22705.
33. Wallberg, A.E., Pedersen, K., Lendahl, U., and Roeder, R.G. (2002). p300 and PCAF Act Cooperatively To Mediate Transcriptional Activation from Chromatin Templates by Notch Intracellular Domains In Vitro. Mol Cell Biol *22*, 7812–7819. 10.1128/mcb.22.22.7812-7819.2002.
34. Gomez-Lamarca, M.J., Falo-Sanjuan, J., Stojnic, R., Abdul Rehman, S., Muresan, L., Jones, M.L., Pillidge, Z., Cerda-Moya, G., Yuan, Z., Baloul, S., et al. (2018). Activation of the Notch Signaling Pathway In Vivo Elicits Changes in CSL Nuclear Dynamics. Dev Cell *44*, 611-623.e7. 10.1016/j.devcel.2018.01.020.
35. Oswald Franz and Kovall, R.A. (2018). CSL-Associated Corepressor and Coactivator Complexes. In Molecular Mechanisms of Notch Signaling, B. D. Borggrefe Tilman and Giaimo, ed. (Springer International Publishing), pp. 279–295. 10.1007/978-3-319-89512-3_14.
36. Petcherski, A.G., and Kimble, J. (2000). Mastermind is a putative activator for Notch. Current Biology *10*, R471–R473. 10.1016/S0960-9822(00)00577-7.
37. Rebay, I., Fehon, R.G., and Artavanis-Tsakonas, S. (1993). Specific truncations of Drosophila Notch define dominant activated and dominant negative forms of the receptor. Cell *74*, 319–329. 10.1016/0092-8674(93)90423-N.
38. Fortini, M.E., Rebay, I., Caron, L.A., and Artavanis-Tsakonas, S. (1993). An activated Notch receptor blocks cell-fate commitment in the developing Drosophila eye. Nature *365*, 555–557. 10.1038/365555a0.
39. Struhl, G., and Adachi, A. (2000). Requirements for Presenilin-Dependent Cleavage of Notch and Other Transmembrane Proteins. Mol Cell *6*, 625–636. 10.1016/S1097-2765(00)00061-7.
40. Wachsmuth, M. (2014). Molecular diffusion and binding analyzed with FRAP. Protoplasma *251*, 373–382. 10.1007/s00709-013-0604-x.
41. Liu, H., Dong, P., Ioannou, M.S., Li, L., Shea, J., Pasolli, H.A., Grimm, J.B., Rivlin, P.K., Lavis, L.D., Koyama, M., et al. (2018). Visualizing long-term single-molecule dynamics in vivo by stochastic protein labeling. Proceedings of the National Academy of Sciences *115*, 343–348. 10.1073/pnas.1713895115.

42. Baloul, S., Roussos, C., Gomez-Lamarca, M., Muresan, L., and Bray, S. (2023). Changes in searching behaviour of CSL complexes in Notch active conditions. In prep.
43. Persson, F., Lindén, M., Unoson, C., and Elf, J. (2013). Extracting intracellular diffusive states and transition rates from single-molecule tracking data. Nat Methods *10*, 265–269. 10.1038/nmeth.2367.
44. Mazza, D., Abernathy, A., Golob, N., Morisaki, T., and McNally, J.G. (2012). A benchmark for chromatin binding measurements in live cells. Nucleic Acids Res *40*, e119–e119. 10.1093/nar/gks701.
45. Krejčí, A., and Bray, S. (2007). Notch activation stimulates transient and selective binding of Su(H)/CSL to target enhancers. Genes Dev *21*, 1322–1327. 10.1101/gad.424607.
46. Irgen-Gioro, S., Yoshida, S., Walling, V., and Chong, S. (2022). Fixation can change the appearance of phase separation in living cells. Elife *11*. 10.7554/eLife.79903.
47. Boija, A., Klein, I.A., Sabari, B.R., Dall'Agnese, A., Coffey, E.L., Zamudio, A. V., Li, C.H., Shrinivas, K., Manteiga, J.C., Hannett, N.M., et al. (2018). Transcription Factors Activate Genes through the Phase-Separation Capacity of Their Activation Domains. Cell *175*, 1842-1855.e16. 10.1016/j.cell.2018.10.042.
48. Sönmezer, C., Kleinendorst, R., Imanci, D., Barzaghi, G., Villacorta, L., Schübeler, D., Benes, V., Molina, N., and Krebs, A.R. (2021). Molecular Co-occupancy Identifies Transcription Factor Binding Cooperativity In Vivo. Mol Cell *81*, 255-267.e6. 10.1016/j.molcel.2020.11.015.
49. Tsai, A., Alves, M.R., and Crocker, J. (2019). Multi-enhancer transcriptional hubs confer phenotypic robustness. 10.7554/eLife.45325.001.
50. Kuang, Y., Pyo, A., Eafergan, N., Cain, B., Gutzwiller, L.M., Axelrod, O., Gagliani, E.K., Weirauch, M.T., Kopan, R., Kovall, R.A., et al. (2021). Enhancers with cooperative Notch binding sites are more resistant to regulation by the Hairless co-repressor. PLoS Genet *17*. 10.1371/journal.pgen.1009039.
51. Kawasaki, K., and Fukaya, T. (2023). Functional coordination between transcription factor clustering and gene activity. Mol Cell *83*, 1605-1622.e9. 10.1016/j.molcel.2023.04.018.

52. Erdős, G., Pajkos, M., and Dosztányi, Z. (2021). IUPred3: prediction of protein disorder enhanced with unambiguous experimental annotation and visualization of evolutionary conservation. Nucleic Acids Res *49*, W297–W303. 10.1093/nar/gkab408.
53. Banani, S.F., Lee, H.O., Hyman, A.A., and Rosen, M.K. (2017). Biomolecular condensates: Organizers of cellular biochemistry. Nat Rev Mol Cell Biol *18*, 285–298. 10.1038/nrm.2017.7.
54. Titov, D. V., Gilman, B., He, Q.L., Bhat, S., Low, W.K., Dang, Y., Smeaton, M., Demain, A.L., Miller, P.S., Kugel, J.F., et al. (2011). XPB, a subunit of TFIIH, is a target of the natural product triptolide. Nat Chem Biol *7*, 182–188. 10.1038/nchembio.522.
55. Clark, M.D., Kumar, G.S., Marcum, R., Luo, Q., Zhang, Y., and Radhakrishnan, I. (2015). Molecular Basis for the Mechanism of Constitutive CBP/p300 Coactivator Recruitment by CRTC1-MAML2 and Its Implications in cAMP Signaling. Biochemistry *54*, 5439–5446. 10.1021/acs.biochem.5b00332.
56. Oswald, F., Täuber, B., Dobner, T., Bourteele, S., Kostezka, U., Adler, G., Liptay, S., and Schmid, R.M. (2001). p300 Acts as a Transcriptional Coactivator for Mammalian Notch-1. Mol Cell Biol *21*, 7761–7774. 10.1128/MCB.21.22.7761-7774.2001.
57. Lasko, L.M., Jakob, C.G., Edalji, R.P., Qiu, W., Montgomery, D., Digiammarino, E.L., Hansen, T.M., Risi, R.M., Frey, R., Manaves, V., et al. (2017). Discovery of a selective catalytic p300/CBP inhibitor that targets lineage-specific tumours. Nature *550*, 128–132. 10.1038/nature24028.
58. Kuang, Y., Golan, O., Preusse, K., Cain, B., Christensen, C.J., Salomone, J., Campbell, I., Okwubido-Williams, F. V., Hass, M.R., Yuan, Z., et al. (2020). Enhancer architecture sensitizes cell specific responses to Notch gene dose via a bind and discard mechanism. Elife *9*. 10.7554/eLife.53659.
59. Dobi, K.C., Halfon, M.S., and Baylies, M.K. (2014). Whole-Genome Analysis of Muscle Founder Cells Implicates the Chromatin Regulator Sin3A in Muscle Identity. Cell Rep *8*, 858–870. 10.1016/j.celrep.2014.07.005.
60. Li, X., Liu, M., Ren, X., Loncle, N., Wang, Q., Hemba-Waduge, R.-U.-S., Yu, S.H., Boube, M., Bourbon, H.-M.G., Ni, J.-Q., et al. (2020). The Mediator CDK8-Cyclin

C complex modulates Dpp signaling in Drosophila by stimulating Mad-dependent transcription. PLoS Genet *16*, e1008832. 10.1371/journal.pgen.1008832.

61. Roninson, I.B., Porter, D.C., and Wentland, M.P. (2016). Cdk8-cdk19 selective inhibitors and their use in anti-metastatic and chemopreventative methods for cancer.
62. McDermott, M.S.J., Chumanevich, A.A., Lim, C., Liang, J., Chen, M., Altilia, S., Oliver, D., Rae, J.M., Shtutman, M., Kiaris, H., et al. (2017). Inhibition of CDK8 mediator kinase suppresses estrogen dependent transcription and the growth of estrogen receptor positive breast cancer. Oncotarget *8*, 12558–12575. 10.18632/oncotarget.14894.
63. Lye, C.M., Naylor, H.W., and Sanson, B. (2014). Subcellular localisations of the CPTI collection of YFP-tagged proteins in *Drosophila* embryos. Development *141*, 4006–4017. 10.1242/dev.111310.
64. Lowe, N., Rees, J.S., Roote, J., Ryder, E., Armean, I.M., Johnson, G., Drummond, E., Spriggs, H., Drummond, J., Magbanua, J.P., et al. (2014). Analysis of the expression patterns, subcellular localisations and interaction partners of *Drosophila* proteins using a *pigP* protein trap library. Development *141*, 3994–4005. 10.1242/dev.111054.
65. Helms, W., Lee, H., Ammerman, M., Parks, A.L., Muskavitch, M.A.T., and Yedvobnick, B. (1999). Engineered Truncations in the Drosophila Mastermind Protein Disrupt Notch Pathway Function. Dev Biol *215*, 358–374. 10.1006/dbio.1999.9477.
66. Giaimo, B.D., Oswald, F., and Borggrefe, T. (2017). Dynamic chromatin regulation at Notch target genes. Transcription *8*, 61–66. 10.1080/21541264.2016.1265702.
67. Townson, J.M., Gomez-Lamarca, M.J., Santa Cruz Mateos, C., and Bray, S.J. (2023). OptIC-Notch reveals mechanism that regulates receptor interactions with CSL. Development *150*. 10.1242/dev.201785.
68. Richter, W.F., Nayak, S., Iwasa, J., and Taatjes, D.J. (2022). The Mediator complex as a master regulator of transcription by RNA polymerase II. Nat Rev Mol Cell Biol *23*, 732–749. 10.1038/s41580-022-00498-3.

69. El Khattabi, L., Zhao, H., Kalchschmidt, J., Young, N., Jung, S., Van Blerkom, P., Kieffer-Kwon, P., Kieffer-Kwon, K.R., Park, S., Wang, X., et al. (2019). A Pliable Mediator Acts as a Functional Rather Than an Architectural Bridge between Promoters and Enhancers. Cell *178*, 1145-1158.e20. 10.1016/j.cell.2019.07.011.
70. Soutourina, J. (2018). Transcription regulation by the Mediator complex. Nat Rev Mol Cell Biol *19*, 262–274. 10.1038/nrm.2017.115.
71. Uyehara, C.M., Leatham-Jensen, M., and McKay, D.J. (2022). Opportunistic binding of EcR to open chromatin drives tissue-specific developmental responses. Proceedings of the National Academy of Sciences *119*. 10.1073/pnas.2208935119.
72. Luyties, O., and Taatjes, D.J. (2022). The Mediator kinase module: an interface between cell signaling and transcription. Trends Biochem Sci *47*, 314–327. 10.1016/j.tibs.2022.01.002.
73. Hannon, C.E., and Eisen, M.B. Intrinsic protein disorder is insufficient to drive subnuclear clustering in embryonic transcription factors. 10.1101/2023.03.27.534457.
74. Chen, M., Li, J., Zhang, L., Wang, L., Cheng, C., Ji, H., Altilia, S., Ding, X., Cai, G., Altomare, D., et al. (2023). CDK8 and CDK19: positive regulators of signal-induced transcription and negative regulators of Mediator complex proteins. Nucleic Acids Res. 10.1093/nar/gkad538.
75. Osman, S., Mohammad, E., Lidschreiber, M., Stuetzer, A., Bazsó, F.L., Maier, K.C., Urlaub, H., and Cramer, P. (2021). The Cdk8 kinase module regulates interaction of the mediator complex with RNA polymerase II. Journal of Biological Chemistry *296*. 10.1016/j.jbc.2021.100734.
76. Bonifer, C., and Cockerill, P.N. (2017). Chromatin priming of genes in development: Concepts, mechanisms and consequences. Exp Hematol *49*, 1–8. 10.1016/j.exphem.2017.01.003.
77. Avramova, Z. (2015). Transcriptional “memory” of a stress: Transient chromatin and memory (epigenetic) marks at stress-response genes. Plant Journal *83*, 149–159. 10.1111/tpj.12832.

78. Tehrani, S.S., Mikulski, P., Abdul-Zani, I., Mata, J.F., Siwek, W., and Jansen, L.E. (2023). STAT1 is required to establish but not maintain interferon-γ-induced transcriptional memory . EMBO J. 10.15252/embj.2022112259.
79. Ferraro, T., Esposito, E., Mancini, L., Ng, S., Lucas, T., Coppey, M., Dostatni, N., Walczak, A.M., Levine, M., and Lagha, M. (2016). Transcriptional Memory in the Drosophila Embryo. Current Biology *26*, 212–218. 10.1016/j.cub.2015.11.058.
80. Zhao, Z., Zhang, Z., Li, J., Dong, Q., Xiong, J., Li, Y., Lan, M., Li, G., and Zhu, B. (2020). Sustained TNF-α stimulation leads to transcriptional memory that greatly enhances signal sensitivity and robustness. Elife *9*. 10.7554/eLife.61965.
81. Pourquié, O. (2003). The Segmentation Clock: Converting Embryonic Time into Spatial Pattern. Science (1979) *301*, 328–330. 10.1126/science.1085887.
82. Dreval, K., Lake, R.J., and Fan, H.-Y. (2022). Analyzing the Interaction of RBPJ with Mitotic Chromatin and Its Impact on Transcription Reactivation upon Mitotic Exit. In, pp. 95–108. 10.1007/978-1-0716-2201-8_9.
83. Zacharioudaki, E., Sanjuan, J.F., and Bray, S. (2019). Mi-2/NuRD complex protects stem cell progeny from mitogenic Notch signaling. 10.7554/eLife.41637.001.
84. Jacobs, C.T., Kejriwal, A., Kocha, K.M., Jin, K.Y., and Huang, P. (2022). Temporal cell fate determination in the spinal cord is mediated by the duration of Notch signalling. Dev Biol *489*, 1–13. 10.1016/j.ydbio.2022.05.010.
85. Oldershaw, R.A., Tew, S.R., Russell, A.M., Meade, K., Hawkins, R., McKay, T.R., Brennan, K.R., and Hardingham, T.E. (2008). Notch Signaling Through Jagged-1 Is Necessary to Initiate Chondrogenesis in Human Bone Marrow Stromal Cells but Must Be Switched off to Complete Chondrogenesis. Stem Cells *26*, 666–674. 10.1634/stemcells.2007-0806.
86. Oswald, F., Rodriguez, P., Giaimo, B.D., Antonello, Z.A., Mira, L., Mittler, G., Thiel, V.N., Collins, K.J., Tabaja, N., Cizelsky, W., et al. (2016). A phospho-dependent mechanism involving NCoR and KMT2D controls a permissive chromatin state at Notch target genes. Nucleic Acids Res *44*, 4703–4720. 10.1093/nar/gkw105.
87. Chan, S.K.K., Cerda-Moya, G., Stojnic, R., Millen, K., Fischer, B., Fexova, S., Skalska, L., Gomez-Lamarca, M., Pillidge, Z., Russell, S., et al. (2017). Role of co-

repressor genomic landscapes in shaping the Notch response. PLoS Genet *13*, e1007096. 10.1371/journal.pgen.1007096.

88. Nandagopal, N., Santat, L.A., LeBon, L., Sprinzak, D., Bronner, M.E., and Elowitz, M.B. (2018). Dynamic Ligand Discrimination in the Notch Signaling Pathway. Cell *172*, 869-880.e19. 10.1016/j.cell.2018.01.002.
89. Kageyama, R., Ohtsuka, T., Shimojo, H., and Imayoshi, I. (2008). Dynamic Notch signaling in neural progenitor cells and a revised view of lateral inhibition. Nat Neurosci *11*, 1247–1251. 10.1038/nn.2208.
90. Falo-Sanjuan, J., Lammers, N.C., Garcia, H.G., and Bray, S.J. (2019). Enhancer Priming Enables Fast and Sustained Transcriptional Responses to Notch Signaling. Dev Cell *50*, 411-425.e8. 10.1016/j.devcel.2019.07.002.
91. Drier, Y., Cotton, M.J., Williamson, K.E., Gillespie, S.M., Ryan, R.J.H., Kluk, M.J., Carey, C.D., Rodig, S.J., Sholl, L.M., Afrogheh, A.H., et al. (2016). An oncogenic MYB feedback loop drives alternate cell fates in adenoid cystic carcinoma. Nat Genet *48*, 265–272. 10.1038/ng.3502.
92. Terriente-Felix, A., Li, J., Collins, S., Mulligan, A., Reekie, I., Bernard, F., Krejci, A., and Bray, S. (2013). Notch cooperates with Lozenge/Runx to lock haemocytes into a differentiation programme. Development (Cambridge) *140*, 926–937. 10.1242/dev.086785.
93. Wang, H., Zang, C., Taing, L., Arnett, K.L., Wong, Y.J., Pear, W.S., Blacklow, S.C., Liu, X.S., and Aster, J.C. (2014). NOTCH1–RBPJ complexes drive target gene expression through dynamic interactions with superenhancers. Proceedings of the National Academy of Sciences *111*, 705–710. 10.1073/pnas.1315023111.
94. Larrivée, B., Prahst, C., Gordon, E., del Toro, R., Mathivet, T., Duarte, A., Simons, M., and Eichmann, A. (2012). ALK1 Signaling Inhibits Angiogenesis by Cooperating with the Notch Pathway. Dev Cell *22*, 489–500. 10.1016/j.devcel.2012.02.005.
95. Mittal, S., Subramanyam, D., Dey, D., Kumar, R. V., and Rangarajan, A. (2009). Cooperation of Notch and Ras/MAPK signaling pathways in human breast carcinogenesis. Mol Cancer *8*. 10.1186/1476-4598-8-128.
96. Efron, B., and Tibshirani, R.J. (1994). An introduction to the bootstrap (CRC press).

97. Li, X., Liu, M., Ren, X., Loncle, N., Wang, Q., Hemba-Waduge, R.-U.-S., Yu, S.H., Boube, M., Bourbon, H.-M.G., Ni, J.-Q., et al. (2020). The Mediator CDK8-Cyclin C complex modulates Dpp signaling in Drosophila by stimulating Mad-dependent transcription. PLoS Genet *16*, e1008832. 10.1371/journal.pgen.1008832.
98. Ovesný, M., Křížek, P., Borkovec, J., Švindrych, Z., and Hagen, G.M. (2014). ThunderSTORM: a comprehensive ImageJ plug-in for PALM and STORM data analysis and super-resolution imaging. Bioinformatics *30*, 2389–2390. 10.1093/bioinformatics/btu202.
99. Chenouard, N., Bloch, I., and Olivo-Marin, J. (2013). Multiple Hypothesis Tracking for Cluttered Biological Image Sequences. IEEE Trans Pattern Anal Mach Intell *35*, 2736–3750. 10.1109/TPAMI.2013.97.
100. Persson, F., Lindén, M., Unoson, C., and Elf, J. (2013). Extracting intracellular diffusive states and transition rates from single-molecule tracking data. Nat Methods *10*, 265–269. 10.1038/nmeth.2367.